

Skimming the Surface: Mapping Flood Extent in the Burdekin Basin with RADAR and GIS

By
Myles Burt

*Thesis
Submitted to Flinders University
for the degree of*

Master of Geospatial Information Science

College of Science and Engineering
24th of October, 2023

TABLE OF CONTENTS

TABLE OF CONTENTS	I
ABSTRACT	III
DECLARATION	IV
ACKNOWLEDGEMENTS	V
LIST OF FIGURES	VI
LIST OF TABLES	VII
CHAPTER 1. INTRODUCTION & LITERATURE REVIEW	1
1.1 The Future of Flooding	1
1.2 Flooding in the Lower Burdekin Basin.....	1
1.3 Economic Challenges in Flood Mapping.....	5
1.4 Issues in Mapping and Identifying Flood.....	5
1.5 Using RADAR in Flood Mapping.....	6
1.6 Question & Significance.....	7
1.7 Scope	8
1.8 Overview	10
CHAPTER 2. METHODOLOGY	11
2.1 Study Area.....	11
2.1.1 Location	11
2.1.2 Terrain	11
2.1.3 Climate.....	13
2.1.4 Land Use/Population.....	19
2.2 Identifying a Flood Event	20
2.3 Data Collection	22
2.4 Data Analysis	24
2.4.1 SAR Processing.....	25
2.4.2 SAR Analysis	28
2.4.3 NDWI Method	31
2.4.4 Detecting Flood using Change Detection Methods.....	33
CHAPTER 3. RESULTS	36
3.1 SAR Results.....	36
3.1.1 Area of Binarised SAR Rasters	36
3.1.2 Area of Change Detection Classification from SAR.....	37
3.2 Optical NDWI Results.....	39
3.2.1 Area of Binarised NDWI Rasters.....	39
3.2.2 Area of Change Detection Classification from NDWI.....	39
3.3 Variation in SAR & NDWI Classifications.....	40
CHAPTER 4. DISCUSSION	42
4.1 Limitations	43

4.1.1 Data Limitations	43
4.1.2 Validation Limitations	43
4.1.3 Temporal Limitations.....	43
4.1.4 Challenges Arising from Cloud Contamination	43
4.1.5 Dissimilar Pixel Size.....	44
4.1.6 Temporal Comparison of SAR and Optical Imagery Acquisition	44
4.2 Unexplored Factors for Enhanced Results	46
4.2.1 DEM & Contour Elevation	46
4.2.2 Consideration of Soil Moisture	46
4.2.3 Inclusion of VH Polarisation Band	46
4.2.4 Alternative SAR Sources.....	47
CHAPTER 5. CONCLUSIONS	48
BIBLIOGRAPHY	49
APPENDIX A.....	54
Area of Interest (AOI)	54
APPENDIX B.....	55
Elevation of AOI	55
APPENDIX C.....	56
Basins and Sub-Basins within the AOI	56
APPENDIX D.....	57
Land Use within AOI using 2019 Land Use / Land Cover Classification Data from Sentinel-2 ...	57
APPENDIX E.....	58
Classified Areas of Change Detected in SAR rasters between Pre-flood and Flood	58
APPENDIX F.....	59
Classified Areas of Change Detected in NDWI rasters between Pre-flood and Flood.....	59

ABSTRACT

This study explores the effective utilization of Synthetic Aperture Radar (SAR) data, specifically from Sentinel-1, for flood identification. The research focuses on how the SAR data collection, processing, and analysis can be performed to provide valuable insights on flood scenarios where optical imagery may fall short, and aid in improved preparedness for future floods in a changing climate. Whilst using SAR for flood identification has a proven and demonstrated method found in academic literature, there is limited academic literature focusing on the validation of SAR methods compared to optical methods for flood identification in the field of remote sensing. SAR technology was applied to identify surface water and classify flood areas within the Lower Burdekin Basin during the severe weather event 'Tropical Low 13U' in 2019. This process involved employing the Sentinel Application Platform (SNAP), an open-source toolbox from the European Space Agency, in conjunction with ESRI's ArcGIS Pro. Flood identification using SAR was established through a binary classification method and validated with the Normalised Difference Water Index (NDWI) processed optical imagery. As a result, SAR successfully identified 5.9% of the land as flooded, in comparison to NDWI's 6.5%, resulting in a minimal 0.6% variation in flood results between SAR binary classification and optical NDWI methods. These findings demonstrate SAR's efficacy in flood identification. While optical imagery, especially when processed with the NDWI method, excels in pinpointing flooded areas, SAR showcases remarkable consistency in capturing and analysing flood events. A distinctive advantage of SAR is its ability to penetrate cloud cover, ensuring uninterrupted data capture in adverse weather conditions. With open-access resources like Sentinel-1 and SNAP from the European Space Agency (ESA), SAR data emerges as a crucial component in the development of cost-effective and efficient flood mapping solutions.

DECLARATION

I certify that this thesis does not incorporate without acknowledgment any material previously submitted for a degree or diploma in any university; and that to the best of my knowledge and belief it does not contain any material previously published or written by another person except where due reference is made in the text.

Signed..........

Date.....12/05/2024.....

ACKNOWLEDGEMENTS

I would most of all like to thank Associate Professor David Bruce, for his guidance, support, and most of all patience with me as I undertook this monumental task in my academic career. As much as I wasn't excited for the fortnightly meetings, I'm sure I'll miss them. Hope my chaotic work ethic offered some entertainment and thank you once again.

To Dr Cristina Solorzano Rivas and Professor Adrian Werner, for inspiring the question behind my thesis after allowing me to listen to your thoughts on flood detection and the possibility of using RADAR.

To Associate Professor Graziela Miot da Silva, for organising and coordinating the Major Research Topic I've undertaken for which this thesis is attributed to.

To all my teachers from the College of Science and Engineering's Geospatial Sciences Department, who aside from being helpful, were fun to talk to and I am grateful for the skills I've learnt from them during my time undertaking a Masters in Geospatial Information Science.

To my academic peers in my GIS cohort, who I've shared many newly found grey hairs, late night computer lab sessions and provided me with advice and laughter during this degree.

To my family, Alison, Randall and Olivia Burt for all the unconditional support they've given me, especially during the end of this Thesis. I can't thank you enough.

To my close friends, for their support during my social absence and making the times we had available during my studies exciting, enjoyable, and wild.

To the GIS team at Tetra Tech Coffey, who have been very supportive by offering me the opportunity to test my skills, and teaching me so much. Especially to my supervisor and mentor Maritza Kolega.

To the crew at Officeworks Marion, for their understanding of my academic studies and being such a fun group to work with.

To Flinders University for having this course and giving me the opportunity to explore a field that I find interesting and have now become passionate about.

To open-access geospatial data, the powerhouse behind allowing young professionals like myself the opportunity to try new and exciting things!

LIST OF FIGURES

Figure 1: Burdekin River at Inkerman Bridge - Highest Annual Flood Peaks	2
Figure 2: The Courier-Mail - First Pictures of Home Hill and Ayr Under Water period	3
Figure 3: Inundation of Sugar Cane Crops during Tropical Low 13U.....	4
Figure 4: Burdekin Falls Dam hitting 185% capacity on 06/02/2019 during Tropical Low 13U.....	4
Figure 5: Map of Area of Interest (AOI)	9
Figure 6: Map of AOI Elevation	12
Figure 7: Map of Climate Classifications of Australia.....	13
Figure 8: Map of Seasonal Rainfall Zones of Australia.....	13
Figure 9: Map of Climate Zones based on Temperature and Humidity.....	14
Figure 10: Map of Average annual, seasonal and monthly rainfall maps (April to November - Queensland)	15
Figure 11: Average annual, seasonal and monthly rainfall maps (October to April - Queensland).	16
Figure 12: Map of Observed Southern Hemisphere TC Genesis Counts Across All Seasons	17
Figure 13: Map of Basins and Sub-Basins within the AOI	18
Figure 14: Map of Land Use within AOI using 2019 Land Use / Land Cover Classification Data from Sentinel-2	19
Figure 15: Graph of daily river average height measurements at the Claire River Gauge Station (120006B) between 2010 and 2023	20
Figure 16: Graph of daily river average height levels at the Claire River Gauge Station (120006B) in 2019.....	21
Figure 17: Graph of daily river average height levels at the Claire River Gauge Station (120006B) between 20/01/2019 and 01/03/2019	21
Figure 18: Map of the Path followed by 'Tropical Low 13U' in 2019.....	22
Figure 19: Flowchart detailing the collection process, variety of days of useable imagery, and which SAR and Optical Imagery were selected to best carry out this study.....	24
Figure 20: Flowchart of processing SAR Data using SNAP.....	27
Figure 21: SNAP Histogram Analysis of SAR Data using to ROI Masks to identify a value for binary thresholding	30
Figure 22: Map of Areas of Change Detected in SAR rasters between Pre-flood and Flood	38
Figure 23: Areas of Change Detected in NDWI rasters between Pre-flood and Flood.....	41
Figure 24: Temporal Limitations highlighted through the Graph displaying Water levels accounting for flow increase and decrease in respect to SAR capture dates between 20/01/2019 and 28/02/2019 at the 120006B (Clare Water Gauge)	45

LIST OF TABLES

Table 1: AOI Coordinates.....	11
Table 2: Parameters of SAR data acquired from Sentinel-1	23
Table 3: Date and Time of SAR data acquisition from ASF (24 Hour-Time Format)	23
Table 4: Date and Time of optical satellite imagery acquisition from Planet (24 Hour-Time Format)	24
Table 5: Generating a SAR Product - SNAP Processing Workflow	25
Table 6: RGB Change Detection Method - SNAP Processing Workflow	28
Table 7: RGB Change Detection band order for SAR import in ArcGIS Pro	28
Table 8: Binarization Classification Method - SNAP Processing Workflow	29
Table 9: Binarised SAR Rasters– ArcGIS Pro Workflow	31
Table 10: NDWI Method – ArcGIS Pro Workflow	31
Table 11: Binarised NDWI Rasters – ArcGIS Pro Workflow	32
Table 12: Change Detection Classification – ArcGIS Pro Workflow	33
Table 13: Change Detection Wizard Classification – ArcGIS Pro Workflow.....	34
Table 14: Area of Binary Classifications in SAR Result for Pre-flood.....	36
Table 15: Area of Binary Classifications in SAR Result for Flood	36
Table 16: Area of change detected in classified SAR rasters between Pre-flood and Flood.....	37
Table 17: Area of Binary Classifications in NDWI Result for Pre-flood	39
Table 18: Area of Binary Classifications in NDWI Result for Flood	39
Table 19: Area of change detected in classified in NDWI rasters between Pre-flood and Flood	40
Table 20: Difference in classification of detected change between SAR and NDWI Results	40
Table 21: List of high-resolution SAR satellites.	47

CHAPTER 1. INTRODUCTION & LITERATURE REVIEW

Flooding, a well-known hazard for communities residing near rivers is undergoing a significant transformation in its frequency and intensity over the next three decades. Projections from the National Oceanic and Atmospheric Administration indicate that by 2050, moderately damaging to damaging floods are anticipated to occur approximately 10 times more frequently globally on average than at present. Additionally, local factors may contribute to further intensification of these events (National Oceanic and Atmospheric Administration (NOAA), 2022).

1.1 The Future of Flooding

The escalation of intense rainfall events associated with a warming global climate in the future, will impact on the dynamics of flooding. Severe precipitation events, which are already the primary instigators of floods, will continue to hold this role. What makes them even more influential is their capacity to trigger floods, regardless of the initial soil conditions (Brunner et al., 2021b). This occurs because the sheer volume of water delivered has the capability to rapidly saturate the soil, rendering the soil's prior dryness inconsequential (Brunner et al., 2021b).

In Australia, the CSIRO has acknowledged the escalating intensity of heavy rainfall events. Predicting that intense daily rainfall events, which typically have a one-in-20-year occurrence, may rise to 4-10% under a low emissions scenario where CO₂ concentrations have declined against the predicted trend. Contrasting against a more significant 8-20% under a high emissions scenario by 2050 where CO₂ concentrations have increased against the predicted trend (CSIRO, 2022). According to the Intergovernmental Panel on Climate Change (IPCC), this anticipated increase in heavy rainfall poses an elevated flood risk, particularly for cities, urban areas, and small catchments where extreme rainfall can lead to rapid flash floods within hours or a day (CSIRO, 2022).

Similar meteorological projections have been made for rural areas and expansive river basins, due to a combination of multi-day rainfall events and varying soil moisture conditions, is hampered by its inherent complexity (CSIRO, 2022). Nevertheless, the overarching trend of heightened flood intensity, attributed to a warming climate, has emerged as a growing concern. A concern that has prompted the creation of this study to understand how remote sensing can aid in combating floods within Australia.

1.2 Flooding in the Lower Burdekin Basin

Flooding poses a prevalent issue for residents living near the river outlets of vast drainage basins, like the Burdekin Basin. Situated along the north-eastern coastline of Queensland, the Burdekin Basin sprawls over an area of approximately 130,000 square kilometres (The State of Queensland,

2023). The primary artery of this basin is the Burdekin River, notable as one of Australia's major rivers in terms of discharge volume (Bureau of Meteorology, 2023i).

The townships of Ayr and Home Hill, flanking the Lower Burdekin River's estuary, have a history intertwined with floods. Flooding in the region has been documented as far back as 1911. Over the years, the area has witnessed a total of 10 major flood events, marked by water levels exceeding 12 metres, measured at the Inkerman Bridge (also known as the Burdekin Bridge) (Bureau of Meteorology, 2023h). However, it's noteworthy that even a minor flood classified as water above 9 metres shown by the added orange line in Figure 1 can have a significant impact on local crops. Figure 1 illustrates the historical record of the highest annual flood peaks along the Burdekin River at the Inkerman Bridge (Bureau of Meteorology, 2023h). This visual representation provides insight into the recurring pattern of flooding in the area.

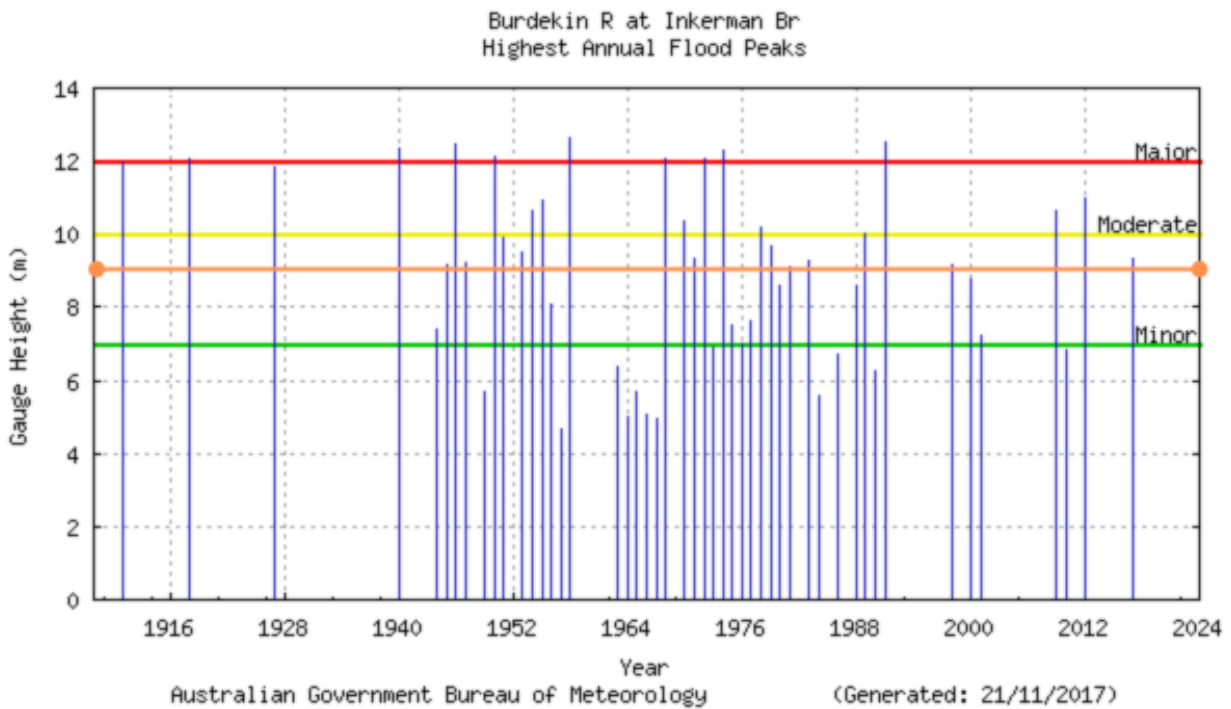


Figure 1: Burdekin River at Inkerman Bridge - Highest Annual Flood Peaks (Bureau of Meteorology, 2023h)

Figure 2 showcases the front page of 'The Courier-Mail' from March 6, 1946, featuring photographs and articles that recount the extensive damage wrought by the flood event on Ayr and Home Hill during that period ("First pictures of Home Hill and Ayr under water," 1946).

Figure removed due to copyright restriction.

**Figure 2: The Courier-Mail - First Pictures of Home Hill and Ayr Under Water period
(1946)**

Figure 3 depicts the inundation of crops such as sugarcane, the predominant agricultural commodity in the Burdekin Local Government Area (LGA), in the aftermath of a flood event (Major, 2019) in 2019. Additionally, Figure 4 highlights the substantial volume of water spilled from Burdekin Falls Dam upstream, that hit 185% capacity on the 6th of February, 2019 (Major, 2019).

Figure removed due to copyright restriction.

**Figure 3: Inundation of Sugar Cane Crops during Tropical Low 13U
(Major, 2019)**

Figure removed due to copyright restriction.

**Figure 4: Burdekin Falls Dam hitting 185% capacity on 06/02/2019 during Tropical Low 13U
(Major, 2019)**

1.3 Economic Challenges in Flood Mapping

Communities such as those in the Lower Burdekin Basin can benefit from flood mapping as it provides invaluable insights for effective flood mitigation but also guides the allocation of resources towards flood protection infrastructure. Furthermore, it informs land use planning and zoning decisions and contributes to advancements in comprehending the causes and consequences of flooding (Kumar et al., 2023).

Flood maps, while essential for risk assessment and mitigation, can be challenging to obtain and comprehend. This complexity can lead to a lack of awareness regarding local flood hazards, potentially fostering a misplaced sense of security within communities. This is especially problematic in areas where effective risk communication and engagement with local authorities are lacking (Auliagisni et al., 2022).

The production and procedures involved in generating flood maps are resource-intensive, which can present economic challenges for communities, particularly in middle to low-income nations. This is largely attributed to the various resources that are required to conduct flood risk mapping, necessitating contributions from professionals across various fields and oversight from governmental authorities (Mohanty and Karmakar, 2022).

Recurring flood events in eastern Australia have spurred the Planning Institute of Australia (PIA) to advocate for a comprehensive framework that incorporates climate change into flood mapping. In Victoria, planners lack access to current and methodologically consistent data on river and coastal inundation. Instead, a fragmented assortment of datasets with differing standards of data collection is maintained, often with uneven application by local councils that may lack the financial resources for essential modelling or the jurisdiction to enforce regulations at the local level (Planning Institute of Australia, 2022). Consequently, flood mapping is not consistently integrated into existing planning controls, and in cases where they are enforced, these controls often fail to address the evolving nature of flood impacts in the context of climate change (Ellis, 2022).

1.4 Issues in Mapping and Identifying Flood

Traditionally, flood mapping relies on ground surveys and aerial observations that can be time-consuming, resource-intensive, and sometimes hazardous due to extreme weather conditions (Liu et al., 2017). As a response, new approaches for monitoring flood impact have emerged, notably hydraulic modelling and remote sensing using optical imagery.

Optical imagery is a popular choice due to its availability of multi-day imagery that produces multispectral data capable of identifying water through calculated indices such as Normalized Difference Water Index (NDWI). NDWI is a remote sensing technique that uses the contrast

between near-infrared and green spectral bands to identify and map water bodies (Liu et al., 2017). Equation 1 displays the equation used in the NDWI method (Gao, 1996b).

$$\text{NDWI} = \frac{(G - \text{NIR})}{(G + \text{NIR})}$$

Equation 1 (Gao, 1996a)

However, optical imagery faces significant challenges in flood mapping, primarily arising from cloud cover and vegetative interference (Shastry et al., 2023).

Clouds frequently obscure optical sensors, making it challenging to obtain clear imagery during flood events. Additionally, optical sensors struggle to differentiate flooded vegetation, leading to a significant drawback in accurately identifying water bodies in the presence of such obstructions. This limitation can result in the underestimation of the extent of inundation during floods (Jones, 2016, Shastry et al., 2023).

Alternatively, hydraulic modelling techniques are frequently employed to predict the extent of inundation, estimate flood depths, and enhance comprehension of riverine and floodplain dynamics (Shastry et al., 2023). Models such as rainfall-runoff models, are designed to simulate the process by which rainfall is transformed into runoff within a catchment area. These models are used in predicting the volume and timing of runoff, making them invaluable for flood forecasting (Kumar et al., 2023).

However, hydraulic models capable of offering intricate insights into flood events often come at a substantial computational cost and may be prone to errors (Shastry et al., 2023). It has been observed that hydraulic models have been shown to underestimate spatial flood dependencies, which depict the relationship between differing geographic locations. Brunner et al. (2021a) highlights a potential gap in how models may not fully capture the intricate ways in which floods spread across different geographic locations, resulting in a lack of spatial coherence in their predictions when compared to observed flood events.

1.5 Using RADAR in Flood Mapping

Gathering high quality and frequent RADAR (Radio Detection and Ranging) data has been known for its high cost and complexity in recent years. However, with the advent of open-access datasets from the European Space Agency's Sentinel-1 satellite, the utilization of RADAR has transitioned into an accessible and enticing opportunity (Flores-Anderson et al., 2019).

RADAR is a key technology in remote sensing, falls under the category of 'Active Remote Sensing.' It operates by utilizing radio-frequency (RF) and electromagnetic (EM) radiation to detect

specific targets. Being an active remote sensor, RADAR has the unique capability to function during both day and night thanks to its use of echolocation principles (Gupta et al., 2022). RADAR performs three fundamental functions (Gupta et al., 2022):

1. Transmitting an EM signal within the RF range toward a target.
2. Receiving a portion of the backscattered signal from the target.
3. Measuring the strength and time delay (phase change) of the backscattered signal that is converted into position and brightness in a digital image for interpretation.

The basic application of RADAR includes Imaging RADAR for capturing images, an Altimeter for measuring surface height variations through time delay, and a Scatterometer for assessing reflectivity concerning the angle of incidence, illumination direction, and polarization. RADAR is generally categorized as Real Aperture RADAR (RAR) and Synthetic Aperture RADAR (SAR) (Gupta et al., 2022).

SAR is a favoured method for flood mapping due to its ability to accurately distinguish between land and water. It commonly utilizes two polarization modes which describe the orientation of the plane of oscillation of a propagating signal: a single polarised sensor supporting only one linear polarisation being vertical transmit and receive (VV) and a single polarised sensor transmitting on linear polarisation and receiving the other being vertical transmit and horizontal receive (VH) for the precise mapping and monitoring of flooding (Parida et al., 2022, Flores-Anderson et al., 2019).

This polarization choice is influenced by the distinct scattering characteristics: VV polarization is particularly effective in capturing rough surface scattering, such as bare ground or water, while VH polarization excels at identifying volume scattering. Volume scattering is indicative of the presence of vegetation or high-penetration soil types like sand (Flores-Anderson et al., 2019).

SAR can effectively detect calm water in both co-polarization and cross-polarization modes through Forward Scattering, indicating minimal or no scattering reflected back to the RADAR antenna. This is typically represented as dark areas in SAR imagery (Gupta et al., 2022).

Flood mapping using SAR offers a solution to the challenges encountered with optical satellite imagery. SAR's unique ability to penetrate cloud cover and, at times, reveal flooding beneath vegetation presents a valuable alternative (Shastry et al., 2023).

1.6 Question & Significance

This study focused on how effectively remotely sensed SAR data can identify flood in comparison to optical imagery methods.

By understanding how to utilise SAR for identifying flooded areas, it can offer crucial insights in flood scenarios where optical imagery falls short, and aid in enhancing the calibration and validation of hydraulic models. Whilst academic literature on the use of SAR data in flood extent

analysis is abundant, literature detailing the comparison of SAR and optical methods for flood extent analysis is limited. Remotely sensed data excels in capturing spatial variability through its consistent spatial coverage and abundant data availability, a significant advantage, especially in regions with limited in-situ data available (Brunner et al., 2021a). This synergy of methods can lead to more realistic flood mapping, achieved through the combination of accessible, achievable, and mutually reinforcing flood mapping techniques and aid in the preparation for future challenges presented by a dynamic and evolving climate.

1.7 Scope

To answer the study question, SAR data will be collected, processed, and analysed over a 760km² area of interest in the Lower Burdekin Basin as seen in Figure 5 and Appendix A. The study will be looking at identifying flood extent by the severe weather event 'Tropical Low 13U', investigating appropriate data between January 1st and February 28th, 2019. Optical imagery obtained for the chosen 'Pre-flood' and 'Flood' dates will be used to compare and validate the effectiveness of SAR results. The 'Pre-flood' date selected was January 7th, 2019 as it contained the best SAR/Optical imagery in moderately dry conditions. The 'Flood' date selected was February 12th, 2019 as it contained the best SAR/Optical imagery after the 'Tropical Low 13U' severe weather event during the date range significant water increases from flooding. The word 'Flood' was used as the imagery illustrated the result of flooding. However, as February 12th, 2019 was not the day flooding peaked, with corresponding imagery captured during the flood decrease, the imagery best represents heavy inundation from resultant flooding. The study is primarily using SAR sourced from Sentinel-1, with processing and classification methods conducted with the Sentinel Application Platform (SNAP), an open-source toolbox provided by the European Space Agency, in conjunction with the closed-source GIS software ArcGIS Pro by ESRI.

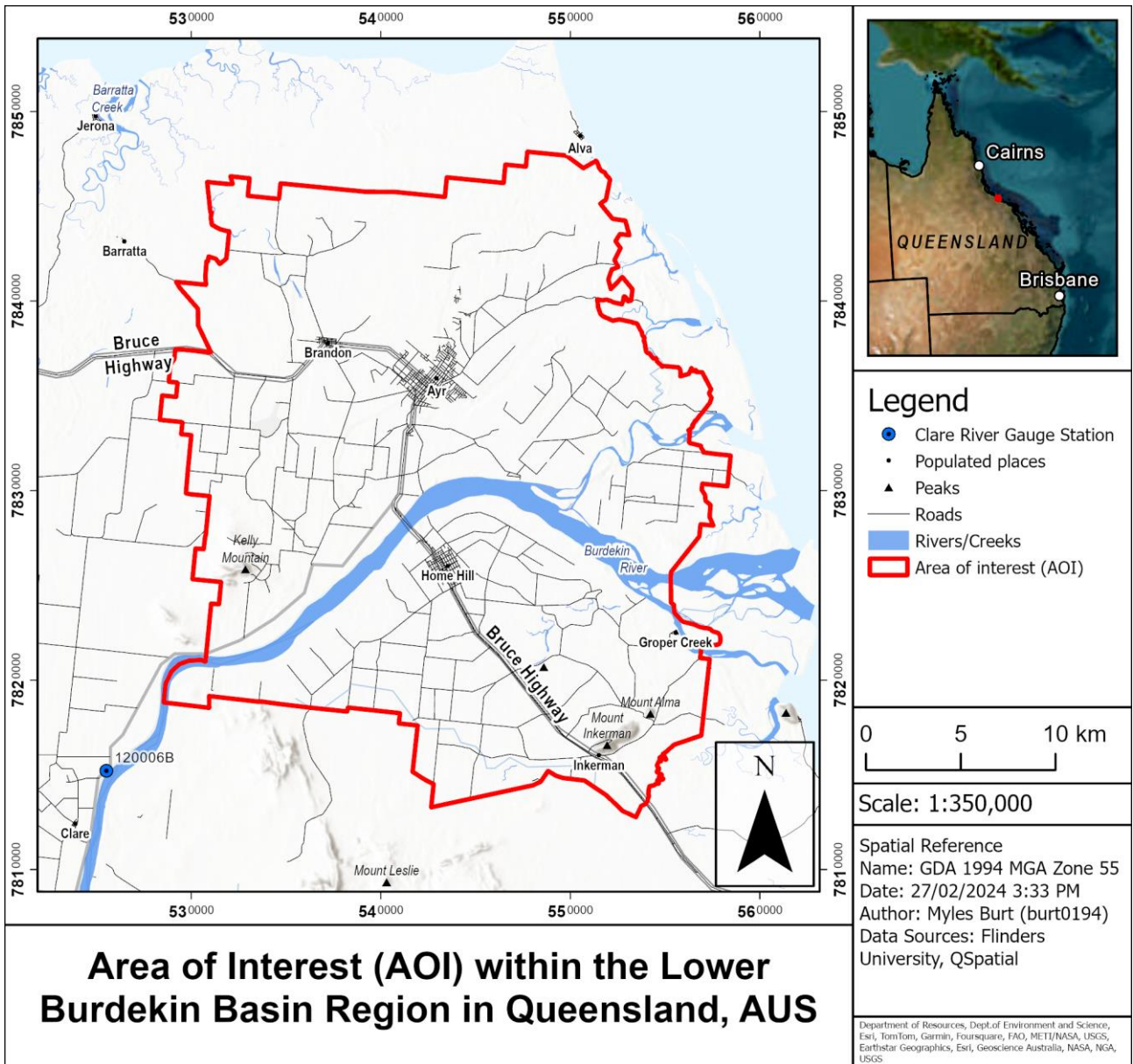


Figure 5: Map of Area of Interest (AOI)

1.8 Overview

In Chapter 2, the research methodology is comprehensively outlined. This begins with an explanation how SAR data is used for the precise identification and classification of water and non-water regions within the designated study area. First, by providing an in-depth description of the study area, including essential details about its geographical location, terrain characteristics, climate conditions, as well as insights into land usage and population within the Area of Interest (AOI) within the Lower Burdekin Basin as seen in Figure 5. The method of selecting the flood event in February 2019, based on an analysis of river height measurements, identifies the 'Tropical Low 13U' monsoon event as flood scenario of interest. The chapter then progresses to discuss data collection, regarding the acquisition of SAR data from the Alaska Satellite Facility (ASF) and optical satellite imagery sourced from Planet. Insights into the rationale behind the selection of specific 'Pre-flood' and 'Flood' dates are explained. The chapter concludes with the methods for data analysis. Detailing the procedure for SAR data pre-processing via the Sentinel Application Platform (SNAP) and introduces two analytical methods: RGB Change Detection and Binarised Classification. The collection of optical imagery in conjunction with the Normalized Difference Water Index (NDWI) for validation is explained. Lastly, the chapter offers insight into the process of flood identification, employing change detection methods on both SAR and NDWI raster outputs.

In Chapter 3, the results from the following methodology are presented. In the SAR data analysis, the extent of surface water and non-water in both pre-flood and flood scenarios are measured, with a focus on a new AOI area of 587.3 square kilometres due to unavailable optical data that would skew the comparison analysis.

In Chapter 4, the results from SAR-processed imagery with those from NDWI-processed optical imagery were discussed.

In Chapter 5, a conclusion is drawn on how SAR data can be collected, processed, and analysed for flood identification in the Lower Burdekin Basin, Queensland, during the 'Tropical Low 13U' monsoon event of early 2019.

CHAPTER 2. METHODOLOGY

To validate the SAR results, optical imagery was collected where available so that a comparison could be made, and the effectiveness of using SAR data to identify flood extent can be understood.

2.1 Study Area

2.1.1 Location

The AOI, a boundary of the Lower Burdekin Water Authority Area, can be located on the north-eastern coastline of Queensland, Australia. Its extent coordinates detailed in Table 1 and encompasses an area of 760km².

Table 1: AOI Coordinates

AOI Coordinates	
<i>GDA 1994 MGA Zone 55 – Metres</i>	
Top - Northern Extent	7,847,881.53 m
Bottom - Southern Extent	7,812,766.49m
Left - Western Extent	528,341.02 m
Right - Eastern Extent	558,459.00 m

2.1.2 Terrain

To understand the terrain of the AOI a 5 metre Digital Terrain Model (DEM) was collected from Geoscience Australia via ELVIS (Geoscience Australia, 2015). The terrain within the AOI is dynamic with an elevation range of -1 to 218m AHD. The reason behind this is the presence of Mount Inkerman and Mount Kelly that both sit above 200m. AOI displays a low elevation of -1m being situated on a coastline and in a river delta. The skew in elevation can be shown as average elevation across the AOI is 8.1m, with the median across all values being 6.5m. The elevation of the AOI is illustrated in Figure 6 and in Appendix B.

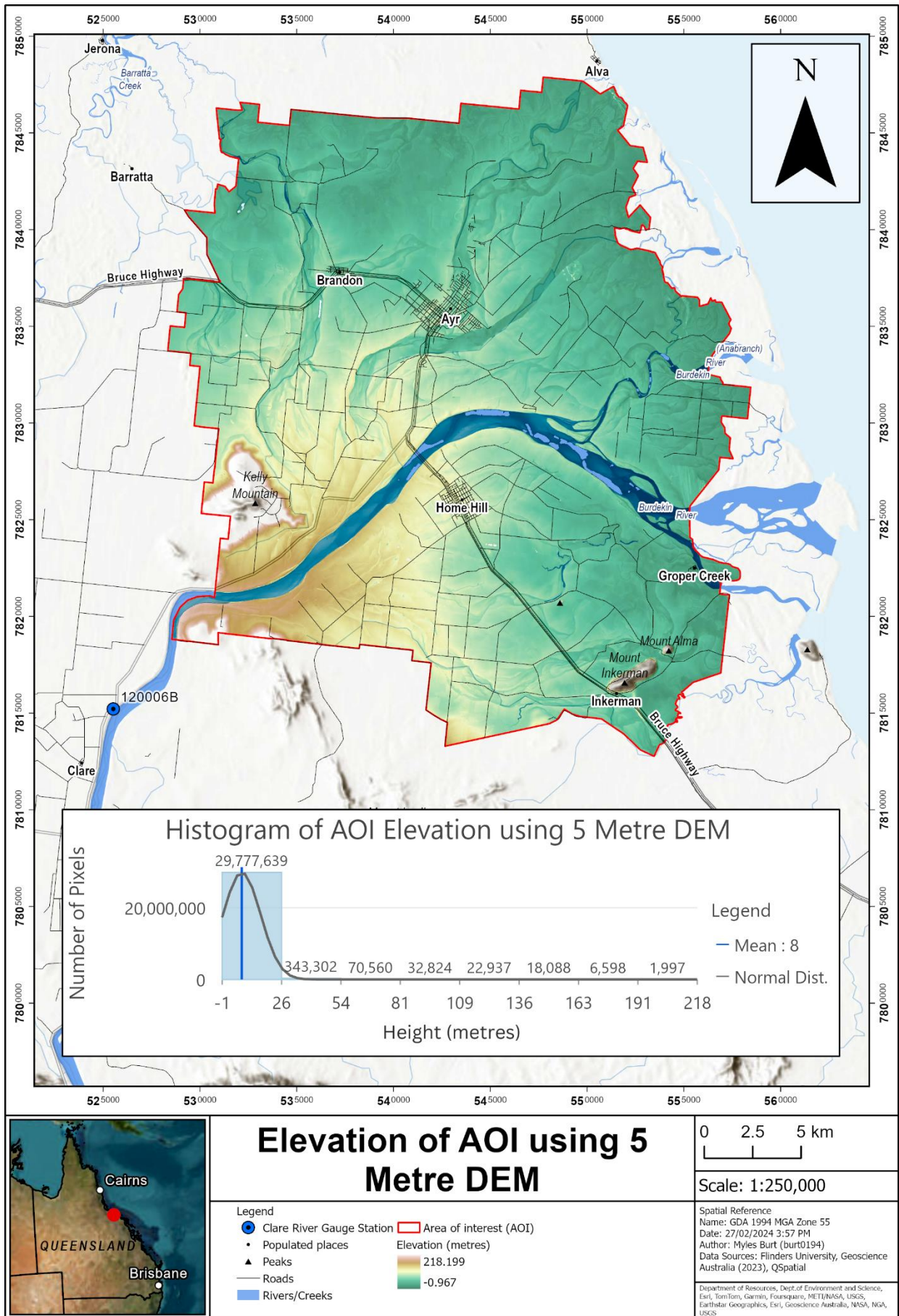


Figure 6: Map of AOI Elevation

2.1.3 Climate

The AOI sits within the Koppen classified areas of Tropical – Savannah. Savannah, abbreviated as ‘Aw’, is described by the precipitation in its driest month being less than 60mm and less than $125 - r$. In the formula ‘r’ represents the mean annual precipitation (Springer Nature, 2023) as shown in Figure 7 The AOI is within a ‘Summer Dominant’ region, marked by its wet summers and dry winters (Bureau of Meteorology, 2023f) as seen in Figure 8

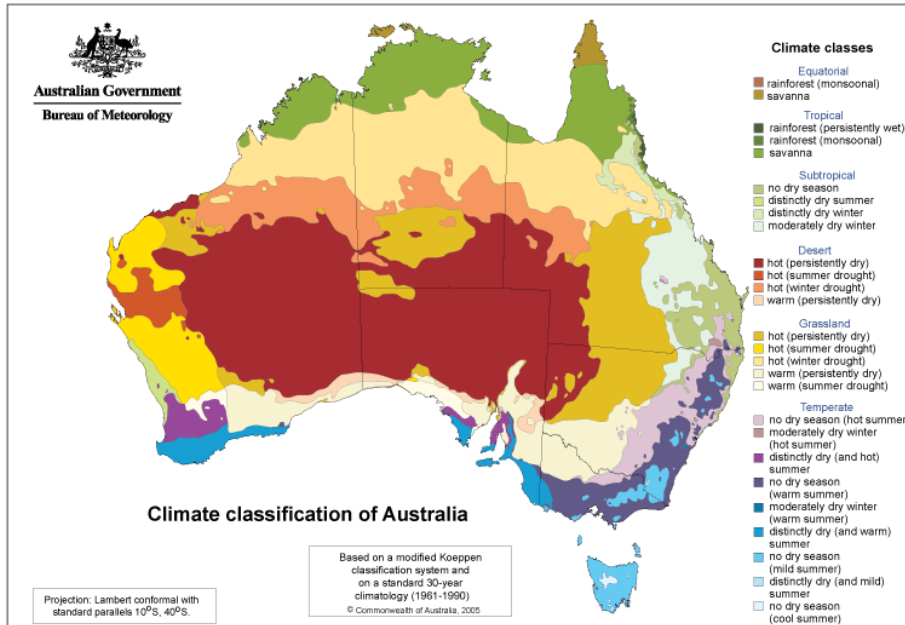


Figure 7: Map of Climate Classifications of Australia (Bureau of Meteorology, 2023e)

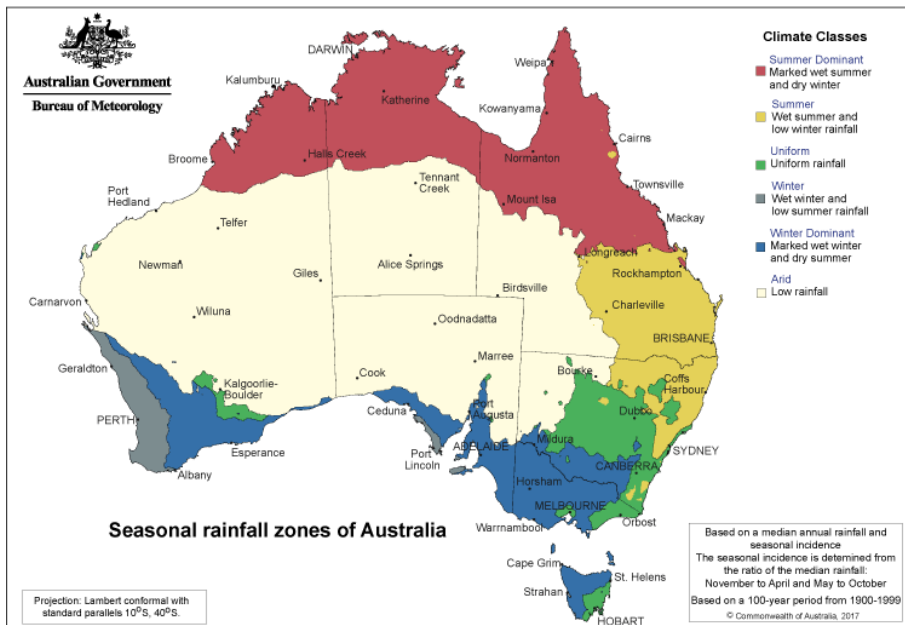


Figure 8: Map of Seasonal Rainfall Zones of Australia (Bureau of Meteorology, 2023f)

Temperature is defined by warm humid summers with the annual mean temperature hitting around 24–27 degrees Celsius (Bureau of Meteorology, 2023g, Bureau of Meteorology, 2023d) as seen in Figure 9 The relative annual humidity ranges from an average of 70-80 percent relative humidity (RH) at 9am (averaged over all Australian Time Zones), and an average of 50-60 RH at 3pm (averaged over all Australian Time Zones), (Bureau of Meteorology, 2023a).

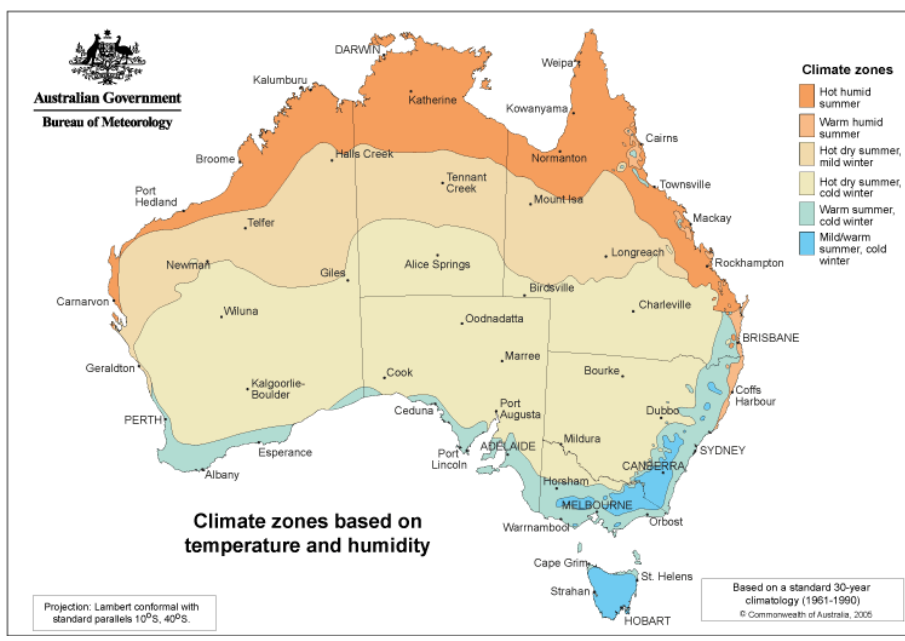


Figure 9: Map of Climate Zones based on Temperature and Humidity (Bureau of Meteorology, 2023g)

Rainfall recorded within the AOI have been averaged at 100-300mm between April to November (Bureau of Meteorology, 2023b) seen in Figure 10 and 600-1200mm between October to April (Bureau of Meteorology, 2023c) seen in Figure 11 These averages highlight the Summer Dominant nature of the region.

Average April to November rainfall 30-year climatology (1991 to 2020)
 Australian Bureau of Meteorology

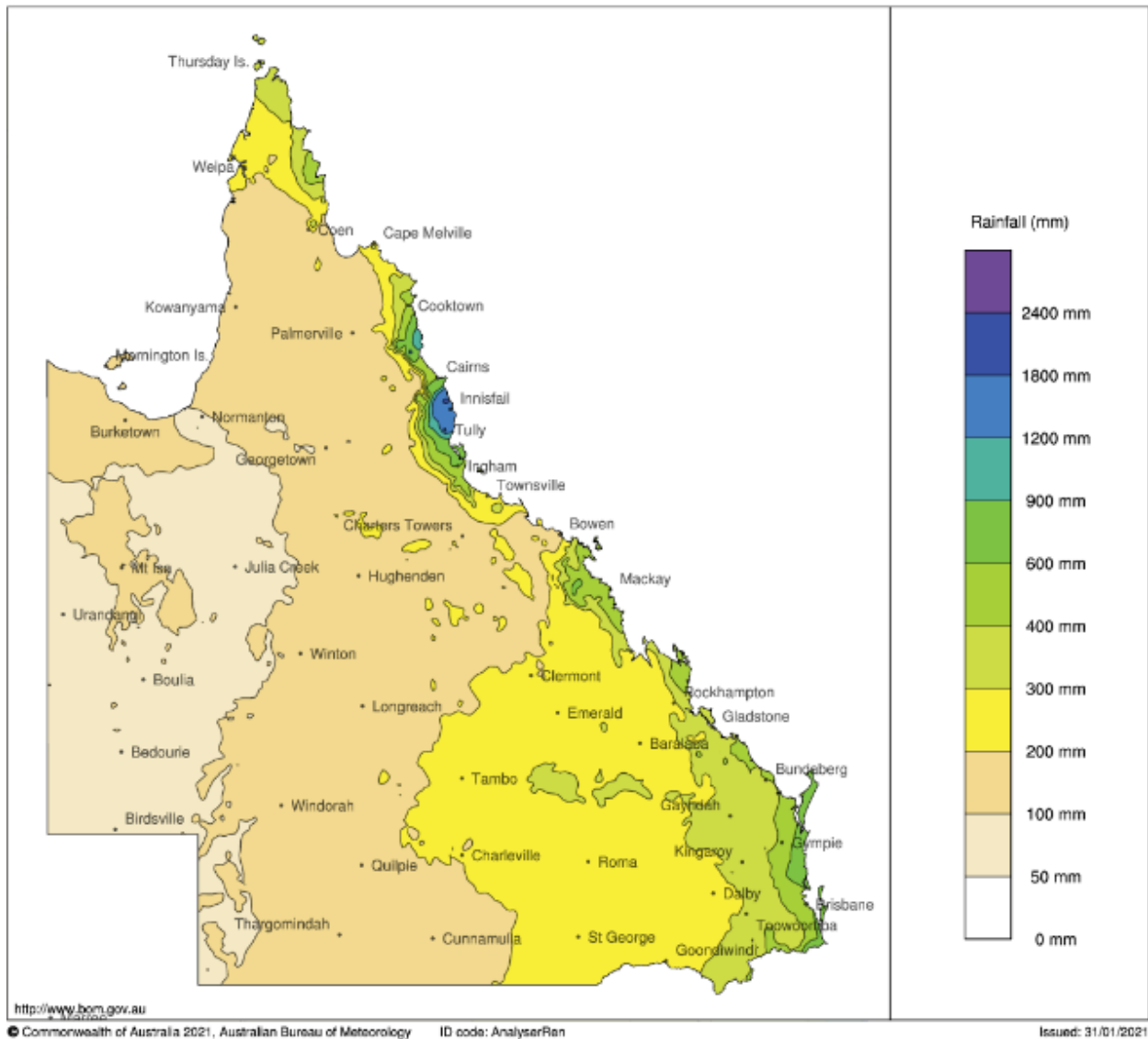


Figure 10: Map of Average annual, seasonal and monthly rainfall maps (April to November - Queensland)
(Bureau of Meteorology, 2023b)

Average October to April rainfall 30-year climatology (1991 to 2020)
 Australian Bureau of Meteorology

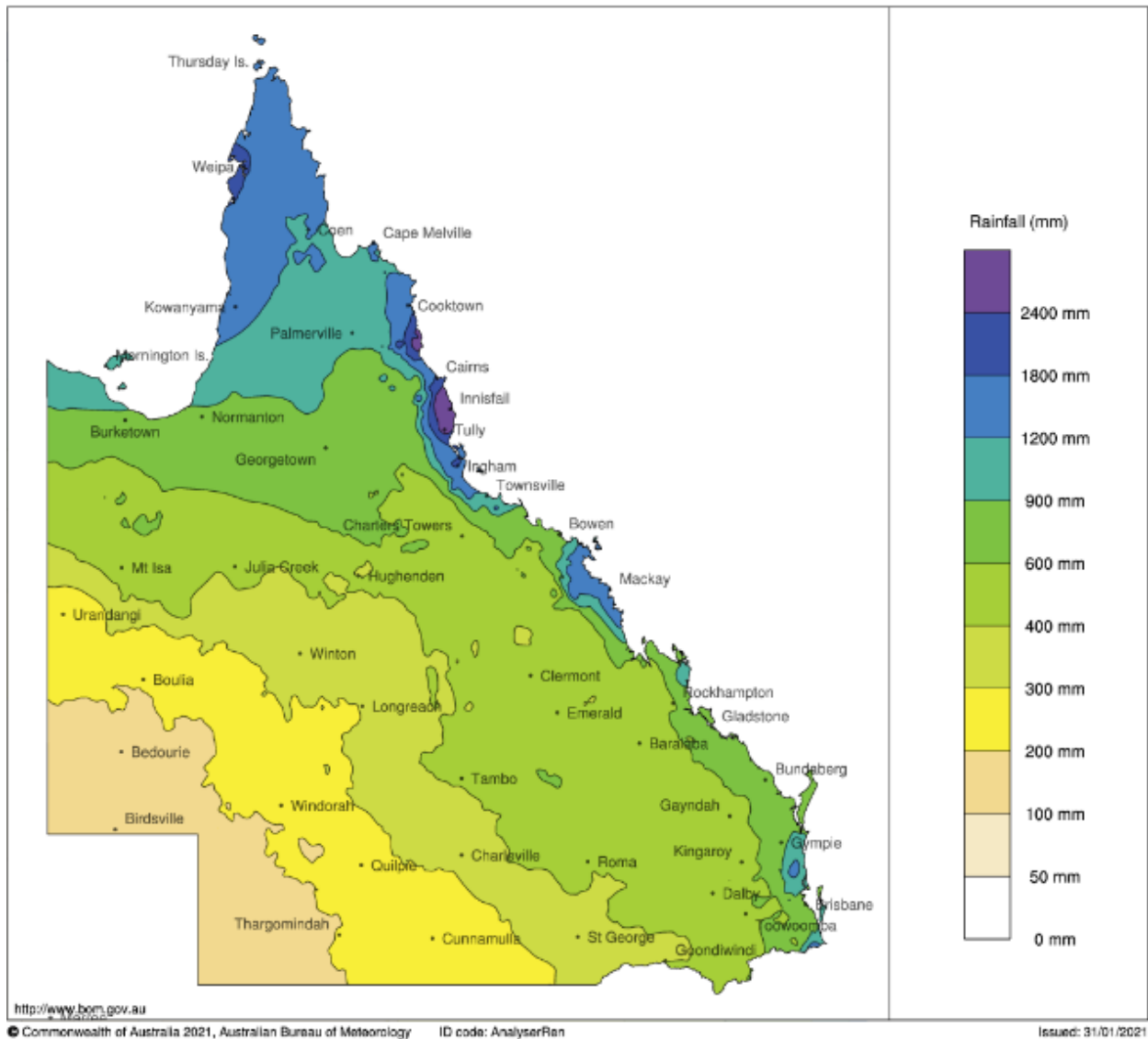


Figure 11: Average annual, seasonal and monthly rainfall maps (October to April - Queensland) (Bureau of Meteorology, 2023c)

The AOI is prone to extreme weather events primarily Tropical Cyclones. The AOI is near a Tropical Cyclone Genesis Count (number of cyclones occurring across all seasons) of around 0.2 to 0.6 as shown in Figure 12 (Bureau of Meteorology, 2023k).

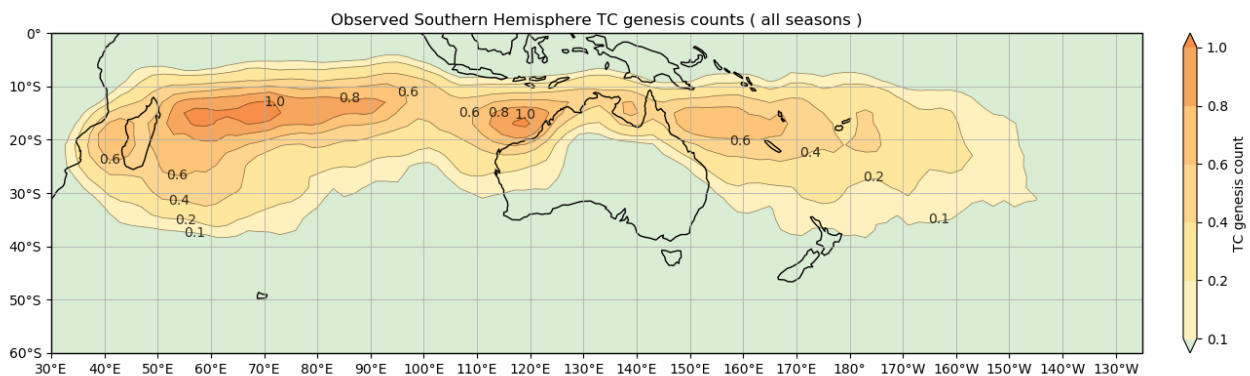


Figure 12: Map of Observed Southern Hemisphere TC Genesis Counts Across All Seasons (Bureau of Meteorology, 2023k)

The AOI holds the Burdekin River, the major river in the AOI and the Mainstem of the Burdekin Basin. The AOI is positioned downstream of the Burdekin River’s three major tributaries being the Suttor River, Bowen River, and Cape River (Bureau of Meteorology, 2023j).

The AOI includes a segment of the Lower Burdekin River that spans three distinct basin and sub-basin regions:

- Burdekin Basin (Lower Burdekin River)
- Haughton Basin (Barratta Creek)
- Don Basin (Don River)

As shown in Figure 13 and in Appendix C.

Flow volume records captured at the Station 120002C in Sellhiem for the 2019-2019 year states that the total annual flow in the Burdekin River at the point was 12,573 gigalitres. More than 2.5 times the average annual value of 4,683 GL with 85 percent of that total occurring in February 2019 (Bureau of Meteorology, 2024).

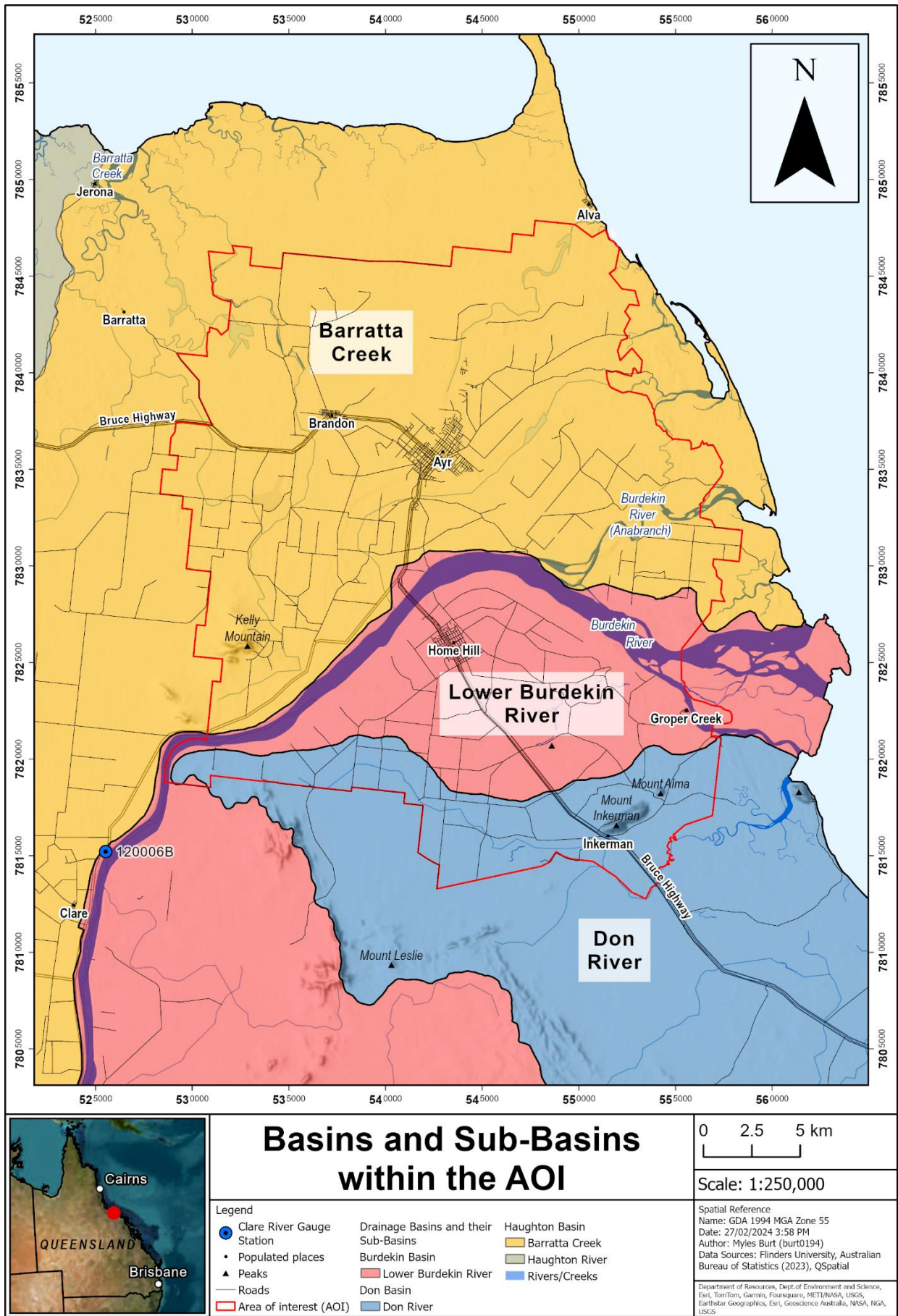


Figure 13: Map of Basins and Sub-Basins within the AOI

2.1.4 Land Use/Population

The AOI resides within the Burdekin Local Government Area (LGA). According to the 2021 Census by the Australian Bureau of Statistics (ABS), the Burdekin LGA holds a population of approx. 16,692 (Australian Bureau of Statistics, 2023). Sugarcane is the prominent industry in the LGA, with sugar cane growing being the highest employed profession, taking up 10.1 percent of employment with 783 people 15 years old and over employed. The second highest is sugar manufacturing, at 8.4 percent with 649 people 15 years old and over employed (Australian Bureau of Statistics, 2023). The major townships in the LGA are Ayr and Home Hill which are also located with the projects AOI (Australian Bureau of Statistics, 2023). Figure 14 and Appendix D. illustrate the land use, major townships, and LGA boundaries within the AOI.

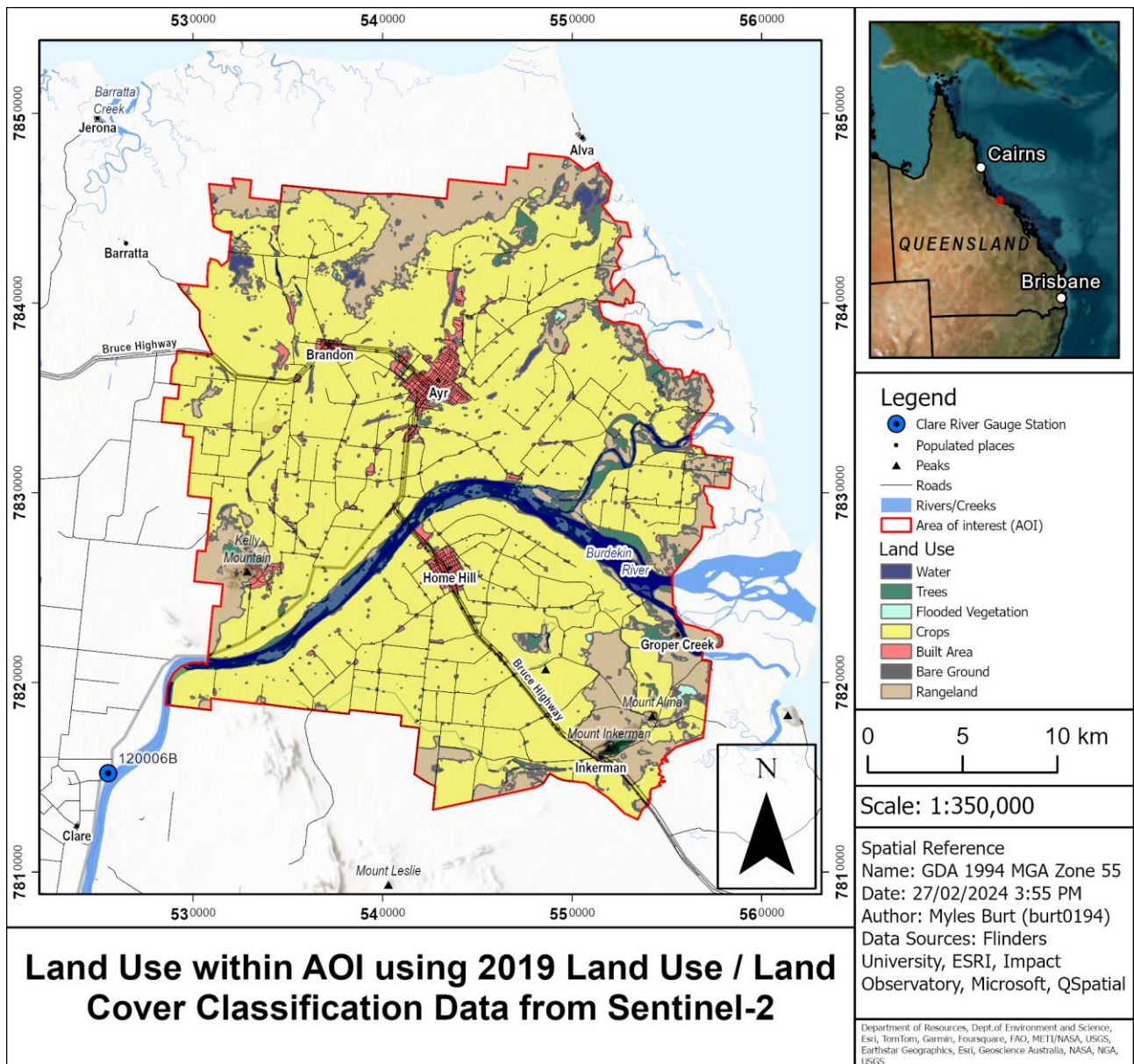


Figure 14: Map of Land Use within AOI using 2019 Land Use / Land Cover Classification Data from Sentinel-2 (ESRI, 2023m)

2.2 Identifying a Flood Event

Accessing the Claire River Gauge Station (120006B) daily river height measurements data, taken at the between 01/10/1974 and 02/03/2023, a suitable time period for the ascertainment of SAR for the project. The Claire River Gauge Station is positioned upstream of the AOI on the Burdekin River at the coordinates 7,815,214°N and 522,521°E (m) (The State of Queensland, 2022).

The gauge station's river height measurements were examined between 2010 and 2023 as seen in Figure 15 The year 2019 was chosen as the best candidate for the project as it displayed the highest water level within the date range, and was within the operational time period of Sentinel-1. The satellite that was chosen to provide SAR data for the project.

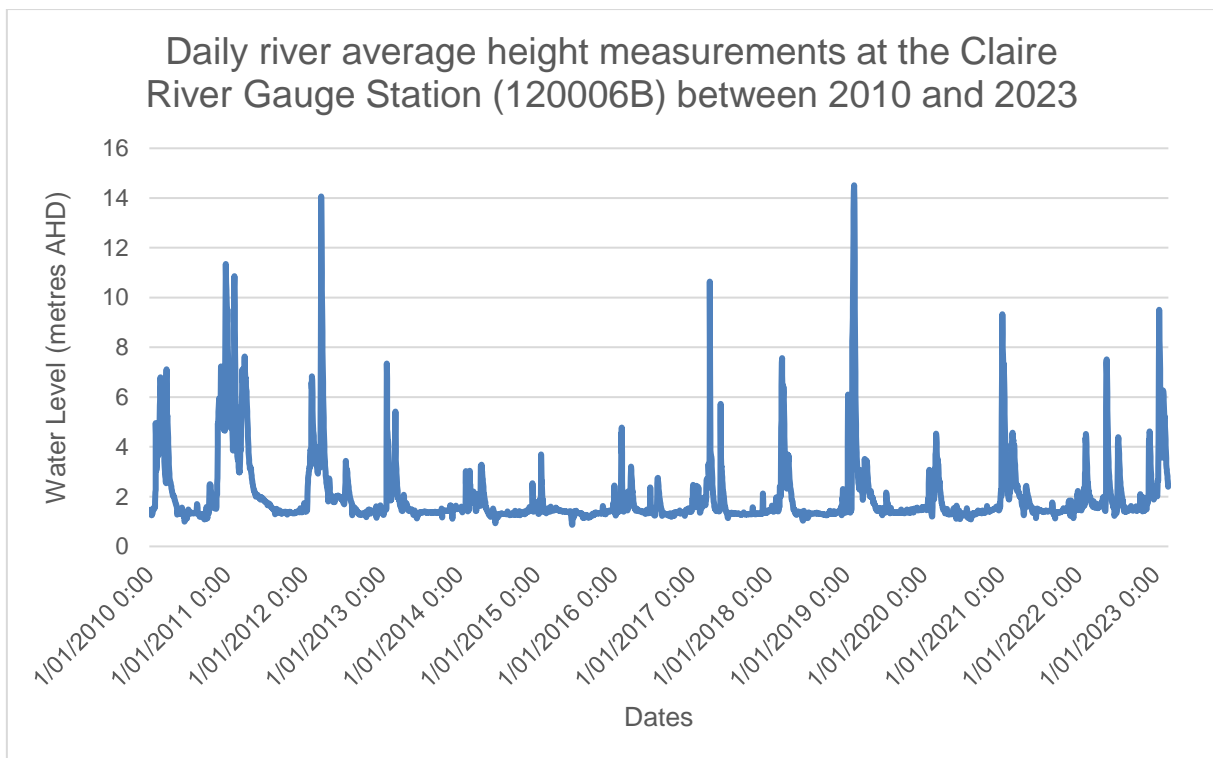


Figure 15: Graph of daily river average height measurements at the Claire River Gauge Station (120006B) between 2010 and 2023

Focusing on the daily river height measurement data from 2019. February was identified as a potential flood event as seen in Figure 16 and further clarified in Figure 17

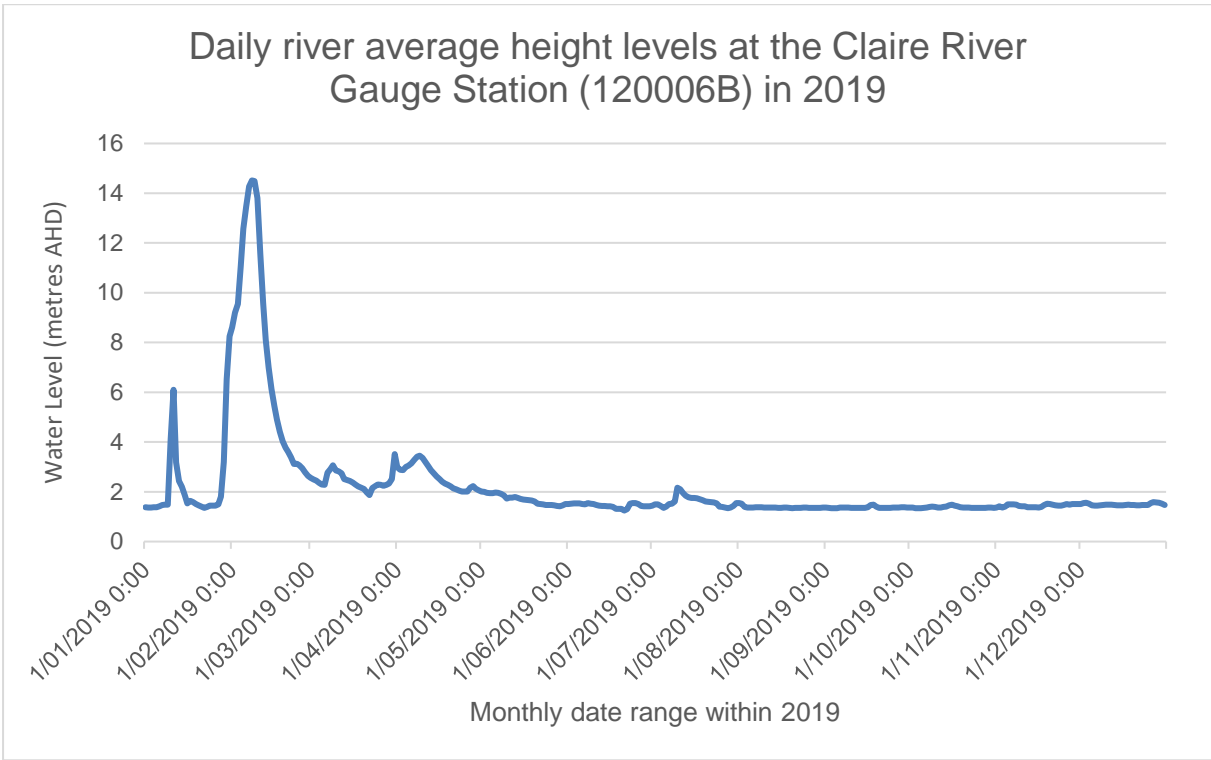


Figure 16: Graph of daily river average height levels at the Claire River Gauge Station (120006B) in 2019

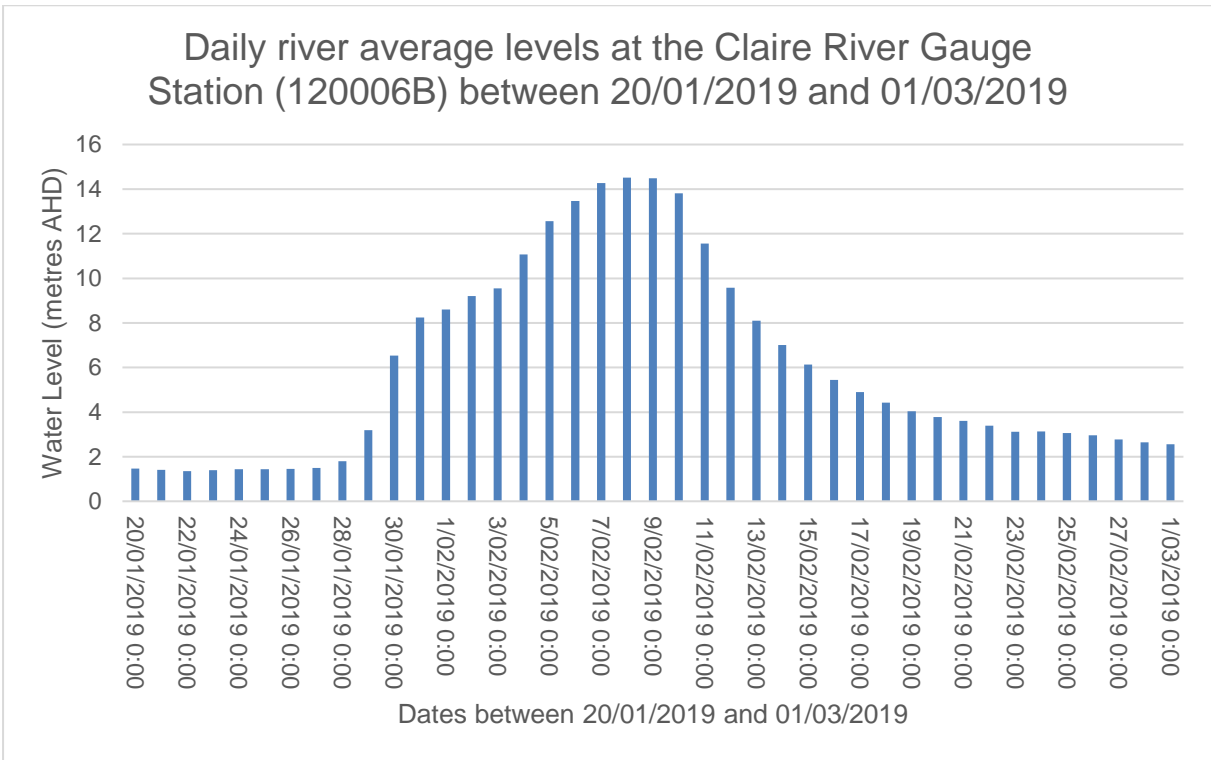


Figure 17: Graph of daily river average height levels at the Claire River Gauge Station (120006B) between 20/01/2019 and 01/03/2019

To confirm if this time period was classified as a flood event, investigation was conducted to identify significant weather events surrounding February, 2019. The cause of the increase in river height recordings during February, 2019 were from a weather event called 'Tropical Low 13U'. A monsoon trough that formed in the Arafura Sea and northern Gulf of Carpentaria, near Cape York Peninsula in Queensland as seen in Figure 18

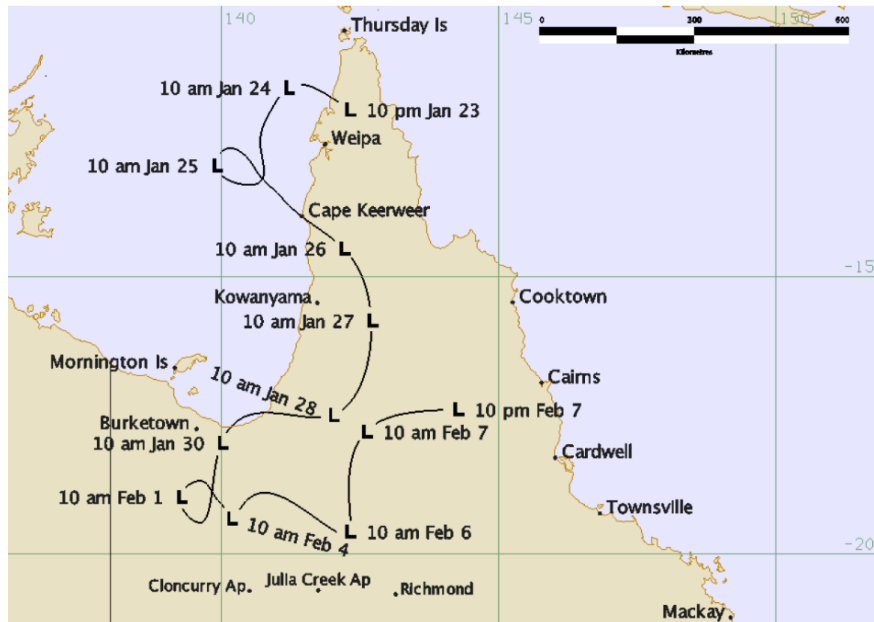


Figure 18: Map of the Path followed by 'Tropical Low 13U' in 2019 (Bureau of Meteorology, 2019)

According to the Australian Bureau of Meteorology (BOM), major flooding occurred in the Burdekin River (Bureau of Meteorology, 2019). By identifying strong evidence of a major flood event in occurring in the AOI in February, 2019. SAR and optical data were then sought in the date ranges of January and February, 2019.

2.3 Data Collection

Through literature review, SAR data was to be acquired as it's widely used to monitor surface water dynamics (Parida et al., 2022). SAR data was collected from the Alaska Satellite Facility's (ASF) Vertex Portal (Alaska Satellite Facility, 2023).

Table 2 details the parameters associated with the data that have been chosen for the study. The VV (vertical transmit and receive) and VH (vertical transmit and horizontal receive) polarisations specifically chosen as they're normally employed for flood mapping (Parida et al., 2022).

Table 2: Parameters of SAR data acquired from Sentinel-1

Satellite	File Type	Beam Mode	Polarisation	Direction	Subtype
Sentinel-1	Ground (GRD)	Interferometric Wide swath (IW)	VH+VV	Descending	SA

Planet Imagery was chosen to provide optical imagery with a pixel resolution of 9 square metres sourced from their 'Dove Classic (PS2)' constellation (Planet, 2023b). This choice was made through its ease of accessibility, friendly user-interface, and cost benefit as 5,000km² is made free for scene downloads per month on an Education and Research Standard plan (Planet, 2023a). The imagery provided was corrected for surface reflectance to include RGB and Near Infrared (NIR) bands so an NDWI could be conducted, and normalised to Sentinel-2 bands for consistent radiometry.

Figure 19 on pg.23 shows the dates SAR and optical data was collected for the study. After examining the product's collected the 7th of January, 2019 was selected as the 'Pre-Flood' date with a recorded river height of 1.5m, and the 12th of February was selected as the 'Flood' date with a recorded river height of 9.6m. The criteria for this choice being:

- SAR and optical imagery needed to be available on the same day for comparison analysis.
- Optical imagery needed to have the best balance between cloud and extent coverage over the AOI.
- Flood date needed to have SAR data and adequate optical imagery available closest to the peak river height recording of 9th of February, 2019 according to 120006B.

The acquisition dates and times for SAR data from ASF and optical satellite imagery from Planet were documented, as illustrated in Tables 3 and Table 4.

Table 3: Date and Time of SAR data acquisition from ASF (24 Hour-Time Format)

Date and Time of SAR data acquisition from ASF (24 Hour-Time Format)		
Category	UTC (Coordinated Universal Time)	AEST (Australian Eastern Standard Time)
Pre-flood	06/01/2019 19:43	07/01/2019 05:43
Flood	11/02/2019 19:43	12/02/2019 05:43

Table 4: Date and Time of optical satellite imagery acquisition from Planet (24 Hour-Time Format)

Date and Time of optical satellite imagery acquisition from Planet (24 Hour-Time Format)		
Category	UTC (Coordinated Universal Time)	AEST (Australian Eastern Standard Time)
Pre-flood	06/01/2019 23:58	07/01/2019 09:58
Flood	11/02/2019 23:56	12/02/2019 09:56

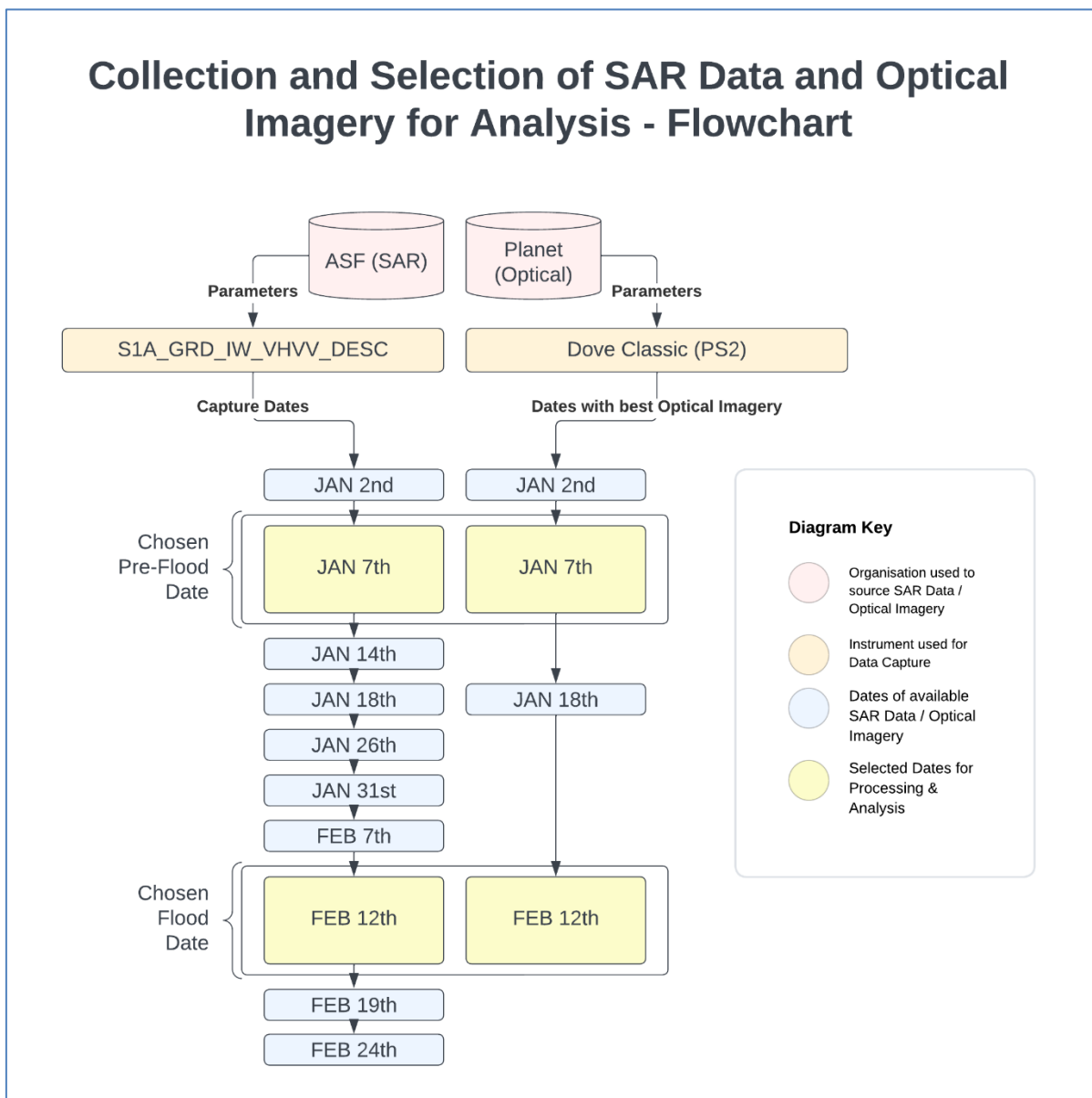


Figure 19: Flowchart detailing the collection process, variety of days of useable imagery, and which SAR and Optical Imagery were selected to best carry out this study.2.4 Data Analysis

2.4.1 SAR Processing

In this study, the Sentinel Application Platform (SNAP) was utilised to process SAR data collected from the ASF. SNAP is an open-source toolbox provided by the European Space Agency (eoPortal, 2023) that was selected due to its widespread use in the field of SAR-based flood mapping (Parida et al., 2022, Wale et al., 2022). Proficiency in using SNAP for SAR-based flood mapping was attained through the study and analysis of educational videos available on YouTube (GIS Appl. in Hydrol. Model. & Remote Sens., 2021a, GIS Appl. in Hydrol. Model. & Remote Sens., 2021b, GIS Appl. in Hydrol. Model. & Remote Sens., 2021c, GIS Appl. in Hydrol. Model. & Remote Sens., 2021d, GIS Appl. in Hydrol. Model. & Remote Sens., 2023a, GIS Appl. in Hydrol. Model. & Remote Sens., 2023b, GIS Appl. in Hydrol. Model. & Remote Sens., 2023c, MrGIS, 2020). These instructional videos served as a valuable foundation, enabling a comprehensive understanding of SNAP. Enabling a comprehensive exploration of the toolbox and enhancing the contextual understanding of existing literature on flood mapping using SAR.

ASF SAR data was imported unzipped into SNAP and via a selection of tools detailed in Table 5. the data was processed for analysis.

Table 5: Generating a SAR Product - SNAP Processing Workflow

Generating a SAR Product - SNAP Processing Workflow	
(GIS Appl. in Hydrol. Model. & Remote Sens., 2021b, GIS Appl. in Hydrol. Model. & Remote Sens., 2021c, MrGIS, 2020)	
Steps	Tool
1.	Apply Orbit File tool was used to update the orbit state vectors in the abstract metadata of the product. The satellite position and velocity information are generally not accurate and can be refined with the inclusion of precise orbit files that are available days-to-weeks after the product is generated.
2.	Thermal Noise Removal tool was used to produce a calibrated noise profile 'de-Noise LUT' from the products noise LUT (Look Up Tables) to remove unwanted interference in the SAR data caused by thermal noise. To improve the quality of the data for further analysis (The European Space Agency, 2023)
3.	Slice Assembly tool is used only if there are two SAR datasets that need to be merged. Slice Assembly combines SAR data with the same product characteristics through a combination of tools such as Include, Merge, and Concatenate. This step

	was not necessary for SAR data collected on the Pre-flood (07/01/2019) or Flood (12/02/2019) dates.
4.	Subset tool was used to crop the SAR data to a smaller area so unnecessary data is included in the processing steps moving forward.
5.	Calibration tool was used directly match the pixel values to its related SAR backscatter scene. This is an important step as calibrated SAR images are essential for the quantitative use of SAR data. This tool was used to produce calibrated Sigma Nought (σ^0) images for the study.
6.	Speckle-Filter tool was used to reduce the amount of 'speckles' in the SAR image, which reduce the quality of the image and make feature interpretations more difficult. Lee Filter with a filter size of 5x5 pixels was chosen for this study. Lee Filter removes the noise by minimising either the mean square error or the weighted least squares estimation (Rana and Suryanarayana, 2019).
7.	Range Doppler Terrain Correction tool was used to adjust the SAR image to closely match its position in over real-world terrain. The tool addresses distortions created by topography and tilt of the satellite sensor that can make areas of the image appear closer or further way than they are in within its actual geography. The study used the default SRTM 3Sec DEM with a Bilinear Interpolation resampling method at 10x10 metres.
8.	Linear to from dB tool was used to convert the values from the SAR image from a Linear scale to a Logarithmic scale being Decibels (dB) for convenience in analysis.

The final processed Sigma0_VV_dB band SAR image was then exported as a GeoTIFF, an image file format containing additional information about its georeferenced and spatial resolution. The VH polarisation was not needed for this process. Figure 20 illustrates the workflow used for processing SAR images in SNAP.

SAR Data Processing Flowchart - SNAP

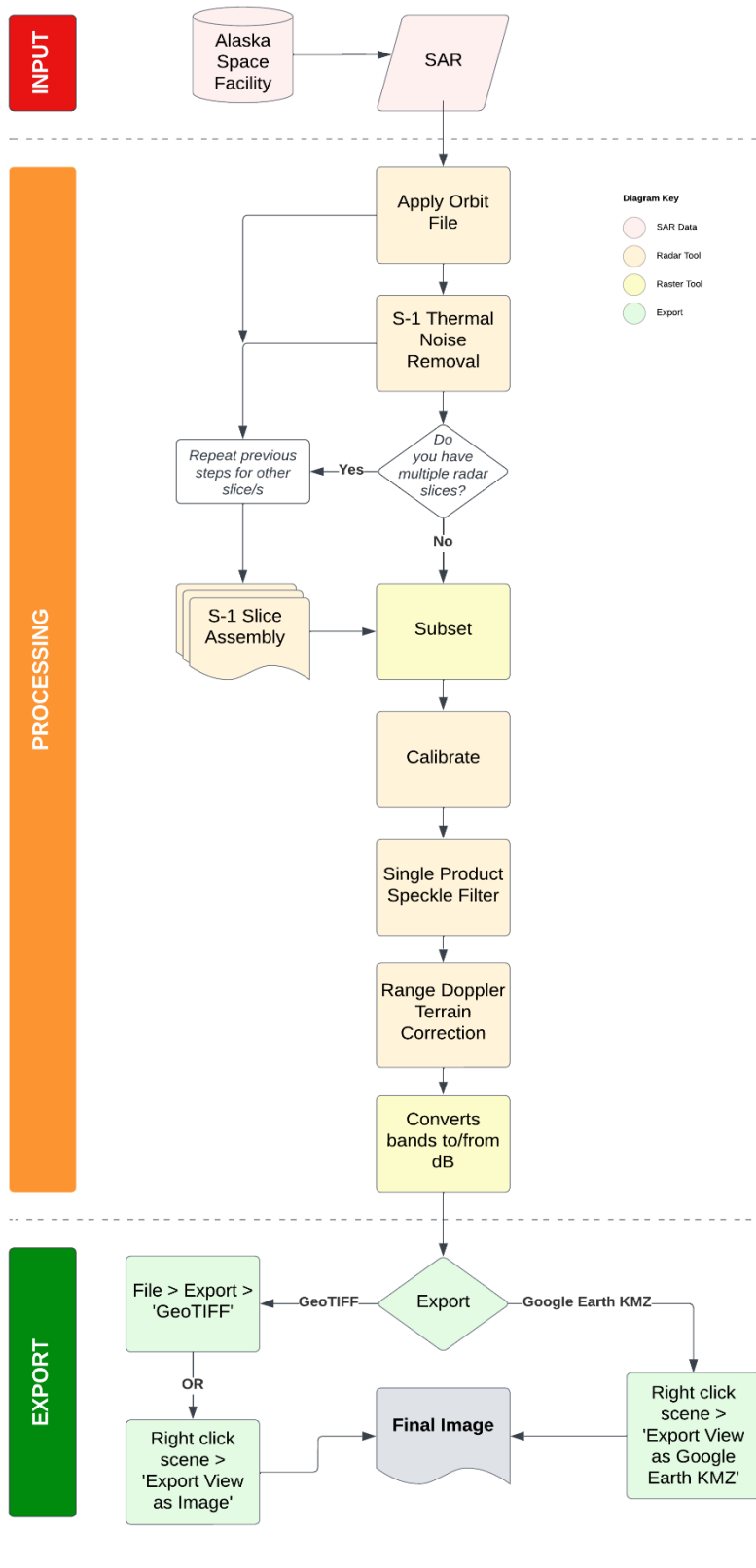


Figure 20: Flowchart of processing SAR Data using SNAP

(GIS Appl. in Hydrol. Model. & Remote Sens., 2021b, GIS Appl. in Hydrol. Model. & Remote Sens., 2021c, MrGIS, 2020)

2.4.2 SAR Analysis

2.4.2.1 RGB Change Detection Method

Within the SNAP software, the SAR data was processed and imported following the procedure outlined in Table 6.

Table 6: RGB Change Detection Method - SNAP Processing Workflow

RGB Change Detection Method - SNAP Processing Workflow	
(GIS Appl. in Hydrol. Model. & Remote Sens., 2021d)	
Steps	Tool
1.	Create Stack , a component of coregistration, is a tool that was used to align two spatially overlapping products. Where the pixel values of one image used as the secondary (mst) are resampled into the geographical raster of the reference image (slv). The Pre-flood SAR image was used as the reference and the Flood SAR image was as the secondary. Resampling was conducted using Bilinear Interpolation.

In the Colour Manipulation window, histogram matching was set to normalise and then RGB Change Detection SAR image was exported as a GeoTIFF. The RGB Change Detection SAR image was imported into ArcGIS Pro, a closed-source GIS software by ESRI. Where the RGB bands where set in accordance to Table 7.

Table 7: RGB Change Detection band order for SAR import in ArcGIS Pro

RGB Change Detection band order for SAR import in ArcGIS Pro	
(GIS Appl. in Hydrol. Model. & Remote Sens., 2021d)	
RGB Bands	RGB Change Detection Band Order
Band 1 (Red)	Pre-flood (slv)
Band 2 (Green)	Flood (mst)
Band 3 (Blue)	Flood (mst)

2.4.2.2 Binarisation Classification Method

Creating a binarised classification between areas of water and non-water was based upon generating a backscattering coefficient (σ^0) off of a bimodal histogram from SAR data in one of the polarisations being VV. Then, determining a threshold value (th) seen as the minimum value on the histogram that separates the two modes. Allowing the construction of a binary mask through $\sigma^0 \leq th$ (Kavats et al., 2022a).

Using the process SAR data, the selected pre-flood and flood raster products underwent a Binarised Classification Method outlined in Table 8.

Table 8: Binarization Classification Method - SNAP Processing Workflow

Binarization Classification Method - SNAP Processing Workflow	
(GIS Appl. in Hydrol. Model. & Remote Sens., 2023a)	
Steps	Tool
1.	<p>New Vector Data Container was used to create two geometries over:</p> <ul style="list-style-type: none"> • Areas containing significant water bodies. • Area with only water.
2.	<p>By employing the Histogram tool within the Analysis ribbon, you can define geometries as 'ROI masks.' This function allows the exclusion of values falling outside the chosen geometries, facilitating the creation of a bimodal histogram for the determination of the threshold value (th).</p> <p>The differentiation between water and land becomes visually apparent through a prominent dip in the bimodal histogram. To enhance the identification of 'th,' a specific geometry can be applied to encompass regions of known water, further refining the bimodal histogram, as depicted in Figure 21.</p>

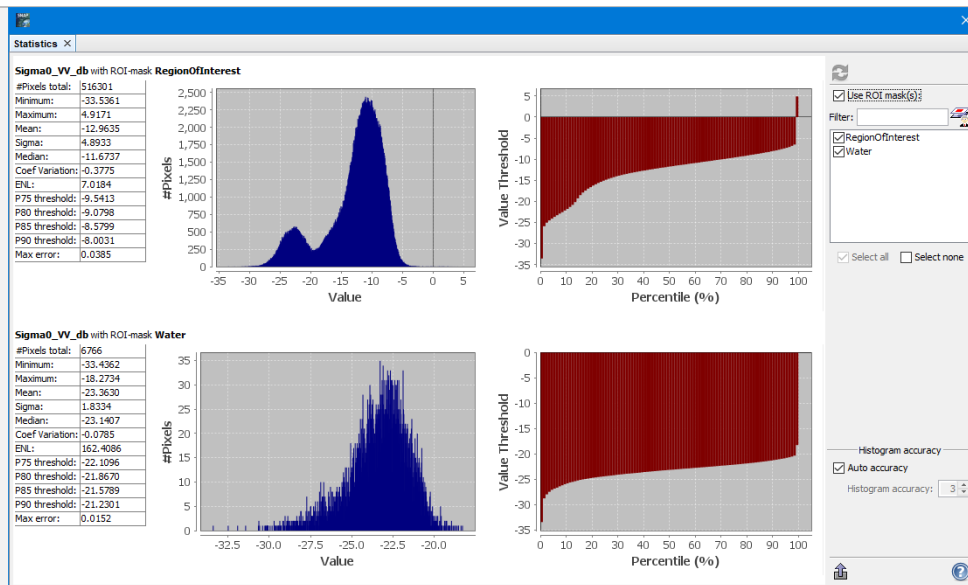


Figure 21: SNAP Histogram Analysis of SAR Data using to ROI Masks to identify a value for binary thresholding

This systematic process enables the estimation of a threshold value crucial for the effective discrimination between water and non-water areas.

- Utilizing the **Band Maths** tool, a technique for generating new image sample values based on existing bands, a binarised classification is derived using the following expression, where ' σ^0 ' is defined as the sigma nought raster, 'th' is defined as the chosen threshold value, and 'NaN' is defined as 'Not a Number':

$$\text{“Raster of interest } (\sigma^0) < \text{threshold value (th) then 1 else NaN”}$$

- Before exporting the data as a GeoTIFF, it's important to note that using Band Maths generates a virtual band, which is essentially a computational representation. To facilitate the export and ensure data storage, this virtual band should be converted into a 'real' band via **Convert Band**.

Once the processing is completed in SNAP, the generated binarised raster can be imported into ArcGIS Pro. Where the raster can be further edited for presentation purposes as outlined in Table 9.

Table 9: Binarised SAR Rasters– ArcGIS Pro Workflow

Binarised SAR Rasters– ArcGIS Pro Workflow	
Steps	Tool
1.	Unnecessary processing can be reduced by utilizing the Clip Raster tool, which allows the extraction of a specific portion of the raster (ESRI, 2023d). Given the irregular polygon shape of the AOI, it's important to enable the "Use input features for clipping" option.
2.	Binarization of the SNAP raster can be done in ArcGIS Pro through the Reclassify tool, which changes the values in the raster into specified classifications (ESRI, 2023i). Natural Break (Jenks) was the chosen, as it creates classes based on the natural groupings inherent in the data (ESRI, 2023e).

2.4.3 NDWI Method

Optical imagery was employed to validate the binarised SAR outcomes through the application of the Normalized Difference Water Index (NDWI) method. The NDWI method computes an index for delineating and monitoring variations in surface water content by utilizing data from the Green and Near Infrared spectral bands (ESRI, 2023h).

Table 10 outlines the workflow used to make an NDWI raster from imported optical imagery collected from the Pre-flood and Flood dates in ArcGIS Pro.

Table 10: NDWI Method – ArcGIS Pro Workflow

NDWI Method – ArcGIS Pro Workflow	
Steps	Tool
1.	Optical imagery is clipped to the AOI using Clip Raster tool (ESRI, 2023d). Given the irregular polygon shape of the AOI, it's important to enable the "Use input features for clipping" option.
2.	To isolate the Green and Near-Infrared (NIR) bands from the raster data, the Make Raster Layer tool is employed to generate a new raster layer for the individual band needed (ESRI, 2023g).

3.	<p>To generate the NDWI raster, the Raster Calculator tool, which enables the creation of a new raster through 'Map Algebra' expressions, is employed (ESRI, 2023k). The formula used in the expression box is as follows:</p> $(float(G-NIR)) / (float(G+NIR))$ <p>The inclusion of 'float' in the expression serves to convert each pixel value of the raster into a floating-point representation (ESRI, 2023f). This conversion is encouraged to prevent potential errors associated with integer-based calculations in future processes.</p>
4.	<p>Utilizing the Project tool, spatial data is transformed from one coordinate system to another (ESRI, 2023j). In this case, the NDWI raster is converted from WGS 1984 to GDA 1994 MGA Zone 55. Additionally, this tool can be harnessed to determine the x and y cell lengths, which are crucial for accurately calculating flood classification areas.</p>

2.4.3.1 Binarised Classification of NDWI Raster

To delineate the boundaries of surface water and non-water areas within the NDWI rasters, a binary classification process was implemented, following the workflow outlined in Table 11.

Table 11: Binarised NDWI Rasters – ArcGIS Pro Workflow

Binarised NDWI Rasters – ArcGIS Pro Workflow	
Steps	Tool
1.	<p>Binarization of the NDWI raster can be done through the Reclassify tool, which changes the values in the raster into specified classifications (ESRI, 2023l). Natural Break (Jenks) was the chosen, as it creates classes based on the natural groupings inherent in the data (ESRI, 2023e).</p> <p>The classification thresholds were established through an iterative process involving the observation of values that most accurately delineated the boundary between surface water and non-water areas. Optical imagery obtained from Planet served as a reference layer for this purpose.</p>

2.4.4 Detecting Flood using Change Detection Methods

2.4.4.1 Classified Change Detection

To measure the changes in SAR and NDWI outputs representing Pre-flood and Flood, the generated rasters are reclassified. This reclassification helps pinpoint specific areas of change, making it possible to calculate the extent of these changes. This process is detailed in Table 12.

Table 12: Change Detection Classification – ArcGIS Pro Workflow

Change Detection Classification – ArcGIS Pro Workflow	
Steps	Tool
1.	Utilizing the Clip Raster tool serves to streamline processing by isolating a defined portion of the raster (ESRI, 2023d). Given the irregular polygon shape of the AOI, it's encouraged to activate the "Use input features for clipping" option.
2.	The Reclassify tool is used to change the values of the rasters into specified binarised classifications (ESRI, 2023l). Natural Break (Jenks) was the chosen, as it creates classes based on the natural groupings inherent in the data (ESRI, 2023e).
3.	<p>The Raster Calculator tool, which allows the creation of a new raster through 'Map Algebra' expressions (ESRI, 2023k) is employed to generate a raster with four classifications. This raster, created by combining the Pre-flood and Flood rasters, categorises areas into the following classes:</p> <ul style="list-style-type: none"> • Always Dry • Flood • False Change (Dry in Flood but Wet in Pre-flood) • Always Wet <p>The conditional statement used for this classification process is as follows:</p> <p style="text-align: center;"><i>Con("Pre-Flood"==1, Con("Flood"==1,5,6), Con("Flood"==1,7,8))</i></p> <p>The logic behind this conditional statement is:</p> <ol style="list-style-type: none"> 1. Look at all data in "Pre-flood". 2. If data in "Pre-flood" is equal to '1': <ul style="list-style-type: none"> • Then, look to the same location in "Flood". If the information in that location is equal to '1', then classify as the number '5'. • If it is not '1', then classify as the number '6'. 3. If data in "Pre-flood" is not equal to '1': <ul style="list-style-type: none"> • Then, look to same location in "Flood". If the information in that location is equal to '1', then classify as the number '7'. • If it is not '1', then classify as the number '8'.

	<p>Using this expression in Raster Calculator, a new raster is created with the following classifications:</p> <ul style="list-style-type: none"> • 5 = “Always Dry” • 6 = “Flood” • 7 = “False Change (Dry in Flood but Wet in Pre-flood)” • 8 = “Always Wet”
4.	<p>Within the new classified raster, the 'Calculate Field' function is employed to determine the values for each field derived from the Raster Calculator (ESRI, 2023a). This process utilizes the pixel dimensions for both the x-axis and y-axis, which are obtained using the Project tool, as detailed in Table 10. The expression for pixel size is:</p> <p style="text-align: center;"><i>Pixel size in m2 = x * y</i></p> <p>This formula computes the area for a single pixel. To determine the total area for each classification in square kilometres (km²), the following expression is used:</p> <p style="text-align: center;"><i>Area in kilometres squared (km2) = (!Count! * (Pixel Size in m2)) / 1e+6</i></p> <p>These calculations are instrumental in quantifying the area for each classification within the raster.</p>

2.4.4.2 Change Detection Wizard Classification

This is used for examining continuous change over an index value rather than categorically. Workflow for this in Table 13.

Table 13: Change Detection Wizard Classification – ArcGIS Pro Workflow

Change Detection Wizard Classification – ArcGIS Pro Workflow	
Steps	Tool
1.	Utilizing the Clip Raster tool serves to streamline processing by isolating a defined portion of the raster (ESRI, 2023d). Given the irregular polygon shape of the AOI, it's encouraged to activate the "Use input features for clipping" option.
2.	The Change Detection Wizard raster function in ArcGIS Pro facilitates a comparative analysis between the Pre-flood and Flood rasters. This process involves identifying the change in pixel values at corresponding locations within both images (ESRI, 2023b).

	<p>The Change Detection Wizard was employed to transform the rasters into a single continuous raster. This process involved four key steps:</p> <ol style="list-style-type: none"> 1. Configuration: The chosen change detection method was 'Pixel Value Change.' This method calculates the differences in pixel values between two continuous rasters. 2. Band Difference: 'Single Band Difference' was the selected band difference method. It calculates the variance in band values for a single band in each raster, considering that each raster is single-banded. 3. Classification of Differences: In this step, the 'Explore Difference Histogram' button was activated, revealing a histogram with approximate minimum and maximum values. The difference values were not rigidly classified, as the goal was to maintain a continuous raster. 4. Output Generation: The 'Smoothing Neighbourhood' was set to 'None.' <p>(ESRI, 2023i)</p> <p>Following these processes, a stretch-based image was generated. It included an index that effectively highlighted pixels with both high and low magnitudes of change.</p>
<p>3.</p>	<p>Within the Symbology pane of the new raster generated by the Change Detection Wizard, a 'Standard Deviation' stretch was configured with two classes (ESRI, 2023c).</p>

CHAPTER 3. RESULTS

3.1 SAR Results

3.1.1 Area of Binarised SAR Rasters

The area of surface water and non-water were measured for the Pre-flood binary classified SAR raster (January 7th, 2019) seen in Table 14 and Flood binary classified SAR raster (February 12th, 2019) seen in Table 15.

The AOI area depicted in these tables is a reflection of the SAR data's pixel size, set at 94 square metres, as it aligns with a predefined polygon shape, thereby yielding an AOI area of approximately 587.3km².

Table 14: Area of Binary Classifications in SAR Result for Pre-flood

Area of Binary Classifications in SAR Result for Pre-flood		
Categories	Area (km ²)	Percentage
Surface Water	6.7	1
Non-Water	580.8	99
AOI	587.3	100

Table 15: Area of Binary Classifications in SAR Result for Flood

Area of Binary Classifications in SAR Result for Flood		
Categories	Area (km ²)	Percentage
Surface Water	51.0	9
Non-Water	536.5	91
AOI	587.3	100

3.1.2 Area of Change Detection Classification from SAR

By employing the methods outlined in Table 16 the classified areas have been created and subsequently quantified.

Table 16: Area of change detected in classified SAR rasters between Pre-flood and Flood

Area of change detected in classified SAR rasters between Pre-flood and Flood		
Categories	Area (km ²)	Percentage
Always Dry	536.0	91
Flood	44.7	8
False Change <i>(Dry in Flood but Wet in Pre-flood)</i>	0.4	0
Always Wet	6.3	1
AOI	587.3	100.00

Maps illustrating the results from Table 16 are presented in Figure 22 and Appendix E.

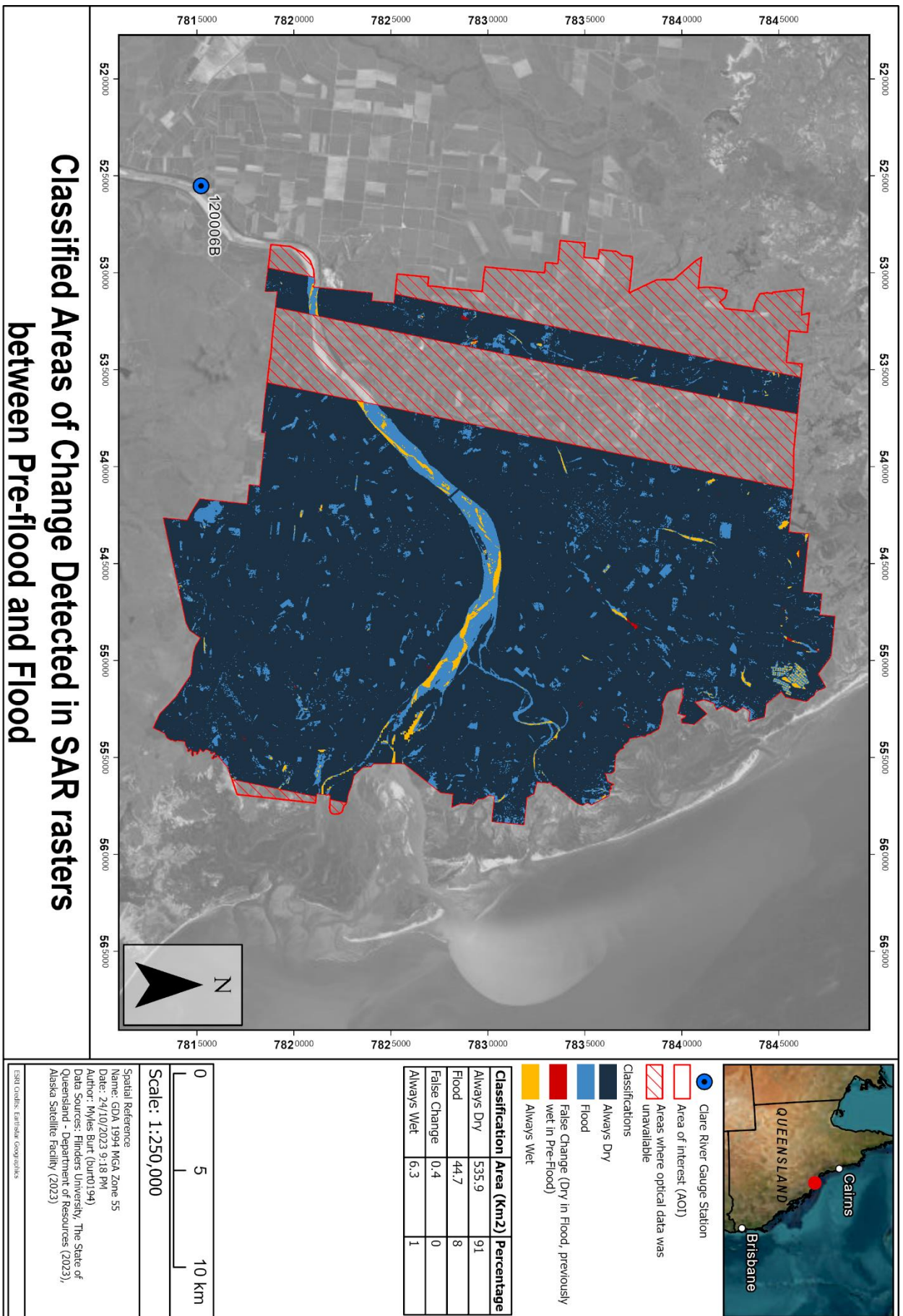


Figure 222: Map of Areas of Change Detected in SAR rasters between Pre-flood and Flood

3.2 Optical NDWI Results

3.2.1 Area of Binarised NDWI Rasters

The area of surface water and non-water were measured for the Pre-flood binary classified NDWI raster (January 7th, 2019) seen in Table 17 and Flood binary classified NDWI raster (February 12th, 2019) seen in Table 18.

The AOI area depicted in these tables is a reflection of the optical imagery pixel size, set at 9 square metres, as it aligns with a predefined polygon shape, thereby yielding an AOI area of approximately 584.27km².

Table 17: Area of Binary Classifications in NDWI Result for Pre-flood

Area of Binary Classifications in NDWI Result for Pre-flood		
Categories	Area (km ²)	Percentage
Surface Water	17.1	3
Non-Water	567.3	97
AOI	584.3	100

Table 18: Area of Binary Classifications in NDWI Result for Flood

Area of Binary Classifications in NDWI Result for Flood		
Categories	Area (km ²)	Percentage
Surface Water	59.7	10
Non-Water	524.6	90
AOI	584.3	100.0

3.2.2 Area of Change Detection Classification from NDWI

By employing the methods outlined in Table 19 the classified areas have been created and subsequently quantified.

Table 19: Area of change detected in classified in NDWI rasters between Pre-flood and Flood

Area of change detected in classified in NDWI rasters between Pre-flood and Flood		
Categories	Area (km²)	Percentage
Always Dry	518.0	89
Flood	49.2	8
False Change (Dry in Flood but Wet in Pre-flood)	6.6	1
Always Wet	10.5	2
AOI	584.3	100

Maps illustrating the results from Table 19 are presented in Figure 23 and Appendix F.

3.3 Variation in SAR & NDWI Classifications

The variations between SAR and NDWI outcomes were quantified for each classified area, as displayed in Table 20.

Table 20: Difference in classification of detected change between SAR and NDWI Results

Difference in classification of detected change between SAR and NDWI Results		
Categories	Area (km²)	Percentage
Always Dry	18.0	0.8
Flood	4.6	0.7
False Change (Dry in Flood but Wet in Pre-flood)	6.2	3.1
Always Wet	4.2	1.1
TOTAL	33.0	5.7

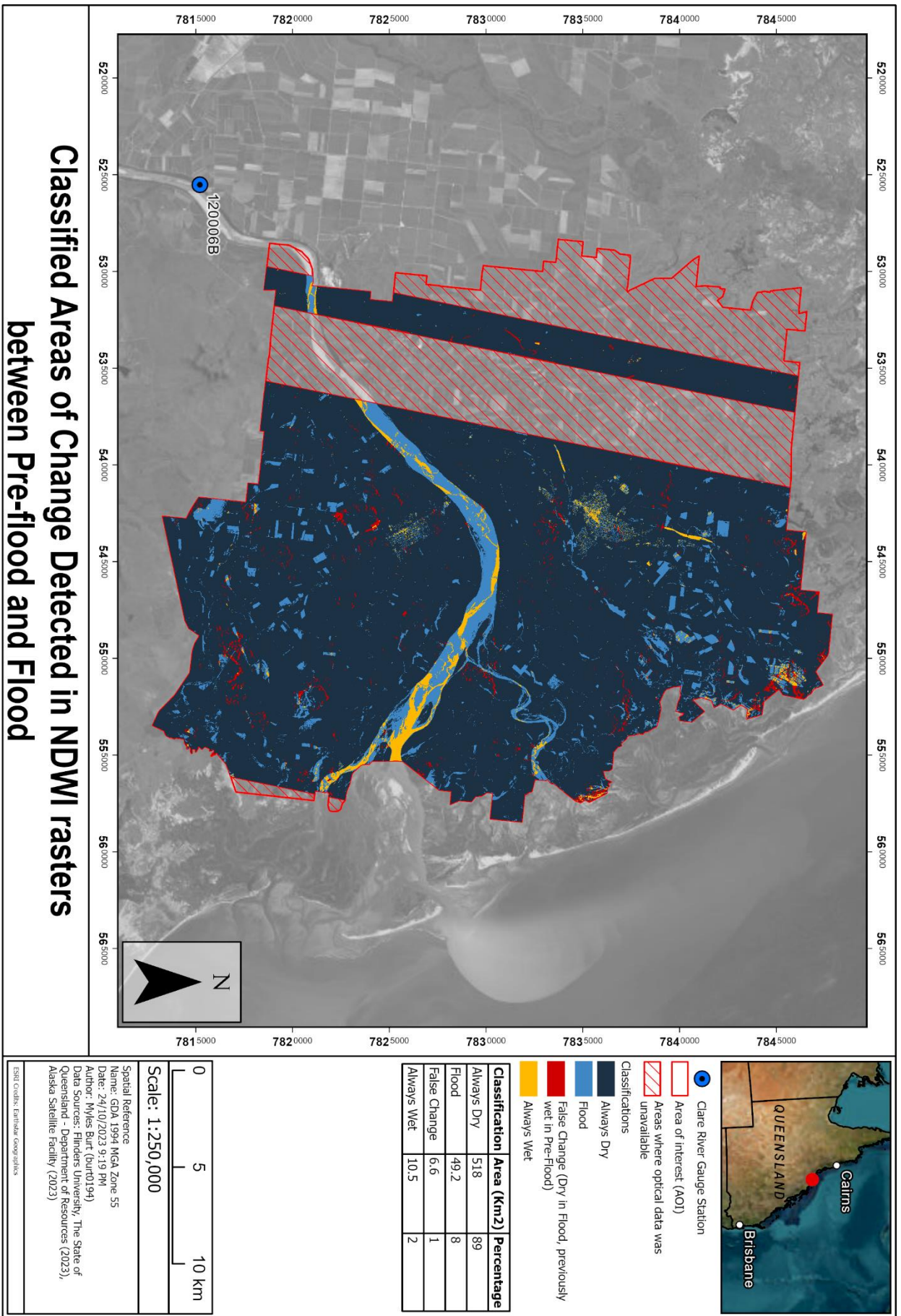


Figure 233: Areas of Change Detected in NDWI rasters between Pre-flood and Flood.

CHAPTER 4. DISCUSSION

When comparing the results of SAR-processed imagery to NDWI-processed optical imagery, the results exhibit a striking similarity, with a minimal variation of 33km² within the defined area of interest (AOI) as seen in Table 20. The results concur with academic literature and what was found in this study.

The consistency in results with the singular use of SAR and NDWI, as observed in various research studies, displays the efficiency of SAR data as a complementary resource in improving flood monitoring techniques. For instance, (Ma et al., 2022) focused on monitoring irrigation events and crop dynamics, the analysis of SAR data from Sentinel-1 and optical imagery from Sentinel-2 revealed a strong correlation between VH/VV polarizations and NDVI/NDWI methods. (Ma et al., 2022) observed a similar correlation was observed when using the VV polarization and NDWI method for this study (Ma et al., 2022).

Furthermore, (Souza et al., 2022) undertook an investigation into environmental and atmospheric influences in SAR and optical imagery utilization for operational reservoir water monitoring emphasized using the VV polarization over VH polarization proved far superior in segmenting water and non-water areas (Souza et al., 2022). The study, which combined SAR data from Sentinel-1 with optical imagery from Landsat-8 and Sentinel-2, found that the accuracy of SAR outputs was comparable with Landsat-8 imagery that had undergone the NDWI process (Souza et al., 2022).

(Notti et al., 2018) explored the potential and limitations of open satellite data for flood mapping using SAR from Sentinel-1 and optical imagery from Landsat-8 and Sentinel-2, acknowledged the challenges posed by factors such as cloud cover, dense urban areas, and forests. However, it demonstrated that by integrating SAR and optical imagery with ancillary data, they were able to achieve highly accurate classifications of inundated areas within their study areas (Notti et al., 2018).

In light of these findings, it becomes evident that the concordance between SAR and NDWI in flood detection highlights the potential of SAR data as a valuable supplementary asset for advancing flood monitoring methodologies. This potential is well exemplified by this study's validation of SAR results through a comparative analysis with NDWI-processed optical imagery.

4.1 Limitations

4.1.1 Data Limitations

The study primarily relied on freely accessible open-source data, with the exception of ArcGIS Pro. Access to higher quality data through proprietary sources may have expanded the scope and accuracy of the analysis. SAR results were generated using integrated STRM 3SEC (90m spatial resolution) Digital Elevation Model (DEM) from SNAP. The utilization of higher-resolution or custom DEMs might have further improved the precision of the SAR data.

The use of SAR and optical data was not optimal for identifying flood as the February 12th "Flood" data was captured after the flood had peaked on February 9th. Freely accessible SAR data for the date of peak flood was not available. SAR data that held more promise of identifying flood extent was recognised as data captured on February 12th. However, this study's aim was to compare and validate the effectiveness of SAR and Optical methods. Usable optical imagery for this date could not be found due to extensive cloud cover.

4.1.2 Validation Limitations

When conducting the study, it did not include the use of hydraulic models or other in situ methods of observation for comparison or validation of SAR results due to awareness and time. The inclusion and validation from ground-based or modelling approaches could have increased the accuracy of the findings as hydraulic models can still provide beneficial results where vegetation and clouds prove an issue in studies using optical and SAR data (Shastry et al., 2023).

Researching the availability/existence of maps illustrating potential flood hazards in the area of interest was overlooked and potentially would have proved beneficial to the study if acquired and included.

4.1.3 Temporal Limitations

It was found during the SAR analysis, that the chosen flood extents did not coincide with the maximum river height measurement recorded during the flood scenario during the study investigation. As a result, the analysis was conducted during a period that might not represent the true peak of the flood. The ability to align SAR data collection precisely through commercial satellite tasking in anticipation of the tropical monsoon event would aid in creating an accurate representation of flood extents.

4.1.4 Challenges Arising from Cloud Contamination

As a result, the most substantial variations were observed within the 'False Change' classification. These differences were primarily due to the presence of clouds that remained in the Pre-flood optical imagery. An inherent limitation of optical imagery lies in its sensitivity to weather conditions during data acquisition, including the potential for cloud cover to obscure water bodies (Li et al., 2021).

Cloud and cloud shadow contamination had a significant impact on the calculation of surface water differences. There was a substantial variation with 61.0% contrast in surface water detection between SAR and NDWI in the Pre-flood imagery, where imagery contained cloud coverage. Contrasting with a significantly decrease of 14.6% in surface water detection in Flood imagery, where no clouds were present.

The disparities in the 'False Change' category further validated these findings, with 1.1% of the classified NDWI result being categorised as false change, compared to 0.1% in the classified SAR result.

4.1.5 Dissimilar Pixel Size

Pixel size played a considerable role in the results. SAR pixels were much larger, covering an area of approximately 94.1 square metres, whereas optical imagery pixels were significantly smaller, at 9 square metres. This inherent difference in pixel size contributed to an issue regarding the variation in the area of interest (AOI) between SAR and NDWI rasters. When attempting to align SAR rasters with a predefined AOI polygon, they covered approximately 587.29 square kilometres, while NDWI rasters encompassed an area of 584.27 square kilometres. This resulted in a minor variation of just 0.5% in the area.

This discrepancy influenced the ability of SAR rasters in detecting subtle changes as it could not identify water in areas such as irrigation canals and small water bodies within the AOI, areas where NDWI rasters excelled.

This concern has been recognized in external research as well. For instance, (Hernandez-Suarez et al., 2022) evaluated the effectiveness of utilizing SAR data from Sentinel-1 and optical imagery from Sentinel-2 to detect aquaculture water bodies identified limitations in water detection primarily stemming from the spatial resolution of the dataset and interference caused by vegetation.

It's noteworthy that optical imagery is highly regarded for its capability to detect small surface water areas. (Souza et al., 2022) revealed that optical imagery consistently outperformed SAR imagery in detecting water features, especially in inlet branches characterized by higher complexity due to diverse water features and the presence of aquatic vegetation.

4.1.6 Temporal Comparison of SAR and Optical Imagery Acquisition

It could be believed that the time of SAR data and optical satellite imagery acquisition could be taken into account for change in pixel classification. Table 3 and Table 4 records the acquisition times for SAR data and optical satellite imagery capture for the Pre-flood and Flood dates. Through this, approx. 4 hours and 15 minutes was the difference between the capture of SAR data and optical imagery.

Given the substantial decline in river height around the selected flood date, displayed in orange in Figure 24 and taking into account the time difference between data captures, it's important to acknowledge that the shifting water bodies during this period could introduce variations in the results between SAR and NDWI classification rasters. Collecting usable optical imagery on the 7th of February, when SAR data was available and flooding peaked, would have likely produced more stable results as the flood heights remained relatively constant during that time period, as evident in Figure 24. displayed in green.

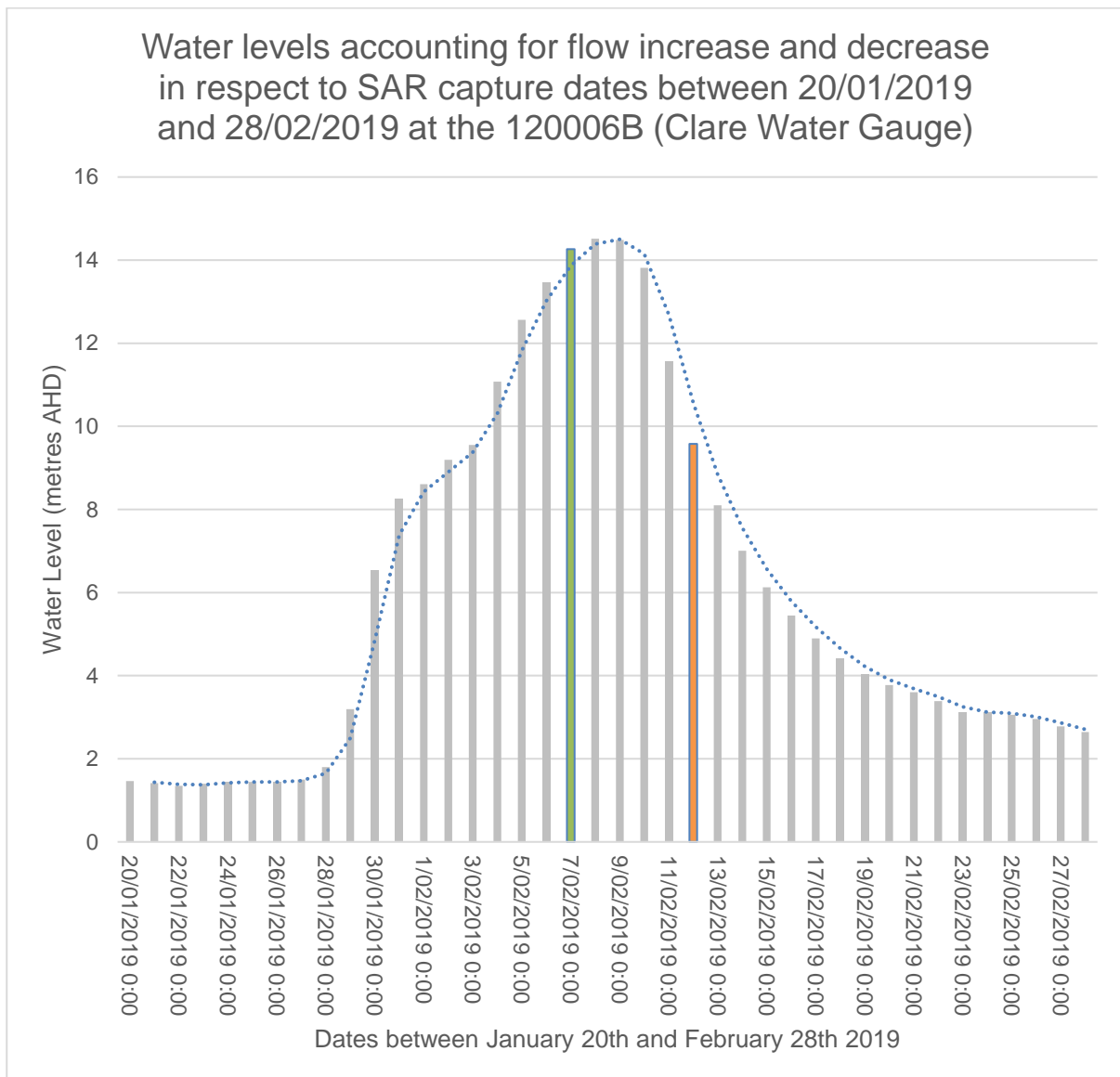


Figure 244: Temporal Limitations highlighted through the Graph displaying Water levels accounting for flow increase and decrease in respect to SAR capture dates between 20/01/2019 and 28/02/2019 at the 120006B (Clare Water Gauge)

4.2 Unexplored Factors for Enhanced Results

4.2.1 DEM & Contour Elevation

Although the SAR data processed in this study using an STRM 3SEC Digital Elevation Model within the SNAP tool, it's important to acknowledge that higher quality open-access DEMs are readily available and could have been employed to enhance the identification of low-lying floodplains and potential sink areas. The use of a high-quality DEM directly impacts the ability to differentiate between urban ground surfaces, roads, and surfaces like airport tarmacs, which exhibit a low backscatter similar to water, thereby reducing the likelihood of misclassification (Konapala et al., 2021). Incorporating the DEM for evaluating elevation contours is advantageous as it helps prevent the misclassification of high-elevation areas as flooded zones (McVittie, 2019).

It's worth emphasizing that elevation plays a significant role in understanding the dynamics of flooding. Therefore, the utilization of a high spatial resolution DEM is highly recommended for more accurate flood monitoring and analysis.

4.2.2 Consideration of Soil Moisture

Incorporating soil moisture data into the study has the potential to enhance the differentiation between water and non-water features. Increased soil moisture content is associated with decreased reflectance, resulting in darker appearances in SAR imagery (Xu et al., 2020). This information can aid in distinguishing genuinely inundated land cover areas from those with high soil moisture content.

4.2.3 Inclusion of VH Polarisation Band

In this study, only the VV polarisation band was employed in flood identification. However, a related study on surface water mapping using SAR images proposed that combining the geometric mean of VV and VH polarisations could lead to a reduction in false positives when constructing threshold masks, compared to using the polarisations separately (Kavats et al., 2022b). This suggestion was grounded in the observation that the geometric mean could raise low sigma nought (σ^0) values that might otherwise be mistakenly interpreted as water, thus contributing to a decrease in false positives during water detection (Kavats et al., 2022b). The study utilized the formula presented in Equation 2 to generate a SAR raster by combining VV (σ^0VV) and VH (σ^0VH) polarisations (Kavats et al., 2022b).

$$\sigma^0VHVV = \sqrt{\sigma^0VH \times \sigma^0VV}$$

Equation 2 (Kavats et al., 2022b)

4.2.4 Alternative SAR Sources

Sentinel-1 was used in this study for capturing SAR data, yet there are other satellites constellations that can produce SAR data within a smaller time frame, and at a higher spatial resolution. Figure 25 lists out a variety of high-resolution SAR satellites (Braun and Hochschild, 2017), that would prove highly beneficial in flood mapping due to its spatial resolution.

Satellite (operator)	Imaging mode (spatial resolution)	Maximum area covered	Time of operation
TerraSAR-X (DLR)	Staring Spotlight (0.6m)	4 x 3.7km	2013 – today
COSMO SkyMed (ASI)	Spotlight-2 (0.8m)	10 x 10km	2007 – today
HRWS (DLR)	StripMap (1m)	70 x 70km	expected 2019
TerraSAR-X (DLR)	Spotlight (1m)	10 x 10km	2007 – today
Radarsat-2 (CSA)	Spotlight (1m)	8 x 18km	2007 - today
Radarsat-2 (CSA)	UltraFine (3m)	20 x 20km	2007 – today
ALOS PALSAR-2 (JAXA)	Spotlight (3m)	25 x 25km	2014 – today
RISAT-1 (ISRO)	FR Stripmap (3m)	25 x 25km	2012 – today
Sentinel-1	StripMap (5m)	80 x 80km	2014 – today

**Table 21: List of high-resolution SAR satellites.
(Braun and Hochschild, 2017)**

Nonetheless, the majority of these satellites are primarily allocated for commercial, scientific, or governmental functions, necessitating requests or payments for access. Companies like ICEYE (ICEYE, 2023) and Capella Space (Capella Space, 2023) are already capable of producing top-tier flood map analyses employing high spatial and temporal resolution SAR imagery. Yet, it's important to note that utilizing such data typically involves fees due to their commercial nature.

CHAPTER 5. CONCLUSIONS

This study conducted quantitative research to investigate how remotely sensed SAR data can be collected, processed, and analysed for flood identification. By identifying and classifying the extent of flooding resulting from the 'Tropical Low 13U' monsoon event that occurred during January and February 2019 within an area of the Lower Burdekin Basin in Queensland, Australia.

This study attempted this through identifying a significant flood event by inspecting river height data obtained from the 120006B stream gauge located upstream of the designated Area of Interest (AOI). Subsequently, Synthetic Aperture RADAR (SAR) data from the Sentinel-1 satellite was procured via the Alaska Satellite Facility (ASF) and processed using the Sentinel Application Platform (SNAP) to generate a refined product suitable for analysis. Using a binarised classification method, the study delineated areas into water and non-water regions, which further resulted in a classified SAR raster that could distinguish between areas of water, flood, non-water, and false change. To validate the SAR results, optical satellite imagery processed with the Normalized Difference Water Index (NDWI) method was obtained. Finally, the study calculated and compared the variations between the SAR and NDWI results, drawing upon similar research for reference.

In conclusion, this study demonstrates the beneficial application of utilizing open-access SAR data for flood identification. While optical imagery, particularly when processed with the NDWI method, can yield superior results in pinpointing flooded areas, SAR exhibits remarkable consistency in capturing and analysing flood events. SAR's standout advantage is its capability to penetrate cloud cover, ensuring uninterrupted data capture in adverse weather conditions. With the accessibility of open-access resources like Sentinel-1 and SNAP through the European Space Agency (ESA), SAR data holds great promise as a crucial component in the development of cost-effective and efficient flood mapping solutions.

Through increased research in methods and techniques to better categorise flood event using open-access SAR data, such advancements will play a pivotal role in the preparation of future climate-related challenges.

BIBLIOGRAPHY

1946. First pictures of Home Hill and Ayr under water. *Courier-Mail (Brisbane, Qld. : 1933 - 1954)*, 06 March 1946.
- ALASKA SATELLITE FACILITY. 2023. *ASF Services – Data Discovery* [Online]. Alaska Satellite Facility. Available: <https://asf.alaska.edu/how-to/data-basics/asf-services-data-discovery/> [Accessed 2023].
- AULIAGISNI, W., WILKINSON, S. & ELKHARBOULTY, M. 2022. Using community-based flood maps to explain flood hazards in Northland, New Zealand. *Progress in Disaster Science*, 14, 100229.
- AUSTRALIAN BUREAU OF STATISTICS. 2023. *Burdekin - 2021 Census All persons QuickStats* [Online]. Australian Bureau of Statistics. Available: <https://www.abs.gov.au/census/find-census-data/quickstats/2021/LGA31900> [Accessed 2023].
- BRAUN, A. & HOCHSCHILD, V. 2017. Potential and Limitations of Radar Remote Sensing for Humanitarian Operations. *Journal for Geographic Information Science*, 1, 228-243.
- BRUNNER, M. I., SLATER, L., TALLAKSEN, L. M. & CLARK, M. 2021a. Challenges in modeling and predicting floods and droughts: A review. *Wiley Interdisciplinary Reviews: Water*, 8, e1520.
- BRUNNER, M. I., SWAIN, D. L., WOOD, R. R., WILLKOFER, F., DONE, J. M., GILLELAND, E. & LUDWIG, R. 2021b. An extremeness threshold determines the regional response of floods to changes in rainfall extremes. *Communications Earth & Environment*, 2, 173.
- BUREAU OF METEOROLOGY. 2019. *Tropical Low 13U – Townsville and northwest Queensland floods* [Online]. Bureau of Meteorology. Available: http://www.bom.gov.au/cyclone/history/Tropical_Low_13U.pdf [Accessed 2023].
- BUREAU OF METEOROLOGY. 2023a. *Average 9 am and 3 pm relative humidity (Annual)* [Online]. Bureau of Meteorology. Available: <http://www.bom.gov.au/climate/maps/averages/relative-humidity/?maptype=09&period=an> [Accessed 2023].
- BUREAU OF METEOROLOGY. 2023b. *Average annual, seasonal and monthly rainfall maps (April to November - Queensland)* [Online]. Bureau of Meteorology. Available: <http://www.bom.gov.au/climate/maps/averages/rainfall/?period=dry®ion=qd> [Accessed 2023].
- BUREAU OF METEOROLOGY. 2023c. *Average annual, seasonal and monthly rainfall maps (October to April - Queensland)* [Online]. Bureau of Meteorology. Available: <http://www.bom.gov.au/climate/maps/averages/rainfall/?period=wet®ion=qd> [Accessed 2023].
- BUREAU OF METEOROLOGY. 2023d. *Average monthly and annual temperature maps (Mean temperature)* [Online]. Bureau of Meteorology. Available: <http://www.bom.gov.au/climate/maps/averages/temperature/?maptype=mean&period=an®ion=qd> [Accessed 2023].
- BUREAU OF METEOROLOGY. 2023e. *Climate classification maps (Koppen - major classes)* [Online]. Bureau of Meteorology. Available: <http://www.bom.gov.au/climate/maps/averages/climate-classification/?maptype=kpngpr> [Accessed 2023].
- BUREAU OF METEOROLOGY. 2023f. *Climate classification maps (Season rainfall - major zones)* [Online]. Bureau of Meteorology. Available: <http://www.bom.gov.au/climate/maps/averages/climate-classification/?maptype=seasgrp> [Accessed 2023].
- BUREAU OF METEOROLOGY. 2023g. *Climate classification maps (Temperature/humidity zones)* [Online]. Bureau of Meteorology. Available: http://www.bom.gov.au/climate/maps/averages/climate-classification/?maptype=tmp_zones [Accessed 2023].
- BUREAU OF METEOROLOGY. 2023h. *FLOOD WARNING SYSTEM for the BURDEKIN RIVER* [Online]. Bureau of Meteorology. Available: <http://www.bom.gov.au/qld/flood/brochures/burdekin/burdekin.shtml#PreviousFlooding> [Accessed 2023].

- BUREAU OF METEOROLOGY. 2023i. *National Water Account 2016* [Online]. Bureau of Meteorology. Available: <http://www.bom.gov.au/water/nwa/2016/burdekin/regiondescription/geographicinformation.shtml> [Accessed 2023].
- BUREAU OF METEOROLOGY. 2023j. *National Water Account 2019 (Burdekin: Geographic information)* [Online]. Bureau of Meteorology. Available: http://www.bom.gov.au/water/nwa/2019/burdekin/regiondescription/geographicinformation.shtml#water_systems [Accessed 2023].
- BUREAU OF METEOROLOGY. 2023k. *Tropical cyclone climatology maps (All years)* [Online]. Bureau of Meteorology. Available: <http://www.bom.gov.au/climate/maps/averages/tropical-cyclones/?period=all> [Accessed 2023].
- BUREAU OF METEOROLOGY. 2024. *Burdekin: Climate and water* [Online]. Bureau of Meteorology,. Available: <http://www.bom.gov.au/water/nwa/2019/burdekin/climateandwater/climateandwater.shtml> [Accessed 2024].
- CAPELLA SPACE. 2023. *SAR Imagery Products* [Online]. Capella Space. Available: <https://www.capellaspace.com/data/sar-imagery-products/> [Accessed 2023].
- CSIRO. 2022. *Understanding the causes and impacts of flooding* [Online]. CSIRO,. Available: <https://www.csiro.au/en/research/natural-disasters/floods/causes-and-impacts> [Accessed 2023].
- ELLIS, M. 2022. *Some councils still rely on outdated paper maps as supercharged storms make a mockery of flood planning* [Online]. The Conversation: The Conversation. Available: <https://theconversation.com/some-councils-still-rely-on-outdated-paper-maps-as-supercharged-storms-make-a-mockery-of-flood-planning-192856> [Accessed 2023].
- EOPORTAL. 2023. *SNAP (Sentinel Application Platform)* [Online]. European Space Agency,. Available: <https://www.eoportal.org/other-space-activities/snap-sentinel-application-platform#snap-sentinel-application-platform-toolbox> [Accessed 2023].
- ESRI. 2023a. *Calculate Field (Data Management)* [Online]. ESRI. Available: <https://pro.arcgis.com/en/pro-app/latest/tool-reference/data-management/calculate-field.htm> [Accessed 2023].
- ESRI. 2023b. *Change Detection Wizard* [Online]. ESRI. Available: <https://pro.arcgis.com/en/pro-app/latest/help/analysis/image-analyst/the-change-detection-wizard.htm> [Accessed 2023].
- ESRI. 2023c. *Change the symbology of imagery* [Online]. ESRI. Available: <https://pro.arcgis.com/en/pro-app/latest/help/data/imagery/symbology-pane.htm> [Accessed 2023].
- ESRI. 2023d. *Clip Raster (Data Management)* [Online]. ESRI. Available: <https://pro.arcgis.com/en/pro-app/latest/tool-reference/data-management/clip.htm> [Accessed 2023].
- ESRI. 2023e. *Data classification methods* [Online]. ESRI. Available: <https://pro.arcgis.com/en/pro-app/latest/help/mapping/layer-properties/data-classification-methods.htm> [Accessed 2023].
- ESRI. 2023f. *Float function* [Online]. ESRI. Available: <https://pro.arcgis.com/en/pro-app/latest/help/analysis/raster-functions/float-function.htm> [Accessed 2023].
- ESRI. 2023g. *Make Raster Layer (Data Management)* [Online]. ESRI. Available: <https://pro.arcgis.com/en/pro-app/latest/tool-reference/data-management/make-raster-layer.htm> [Accessed 2023].
- ESRI. 2023h. *NDWI* [Online]. ESRI. Available: [https://pro.arcgis.com/en/pro-app/latest/arcpy/image-analyst/ndwi.htm#:~:text=The%20Normalized%20Difference%20Water%20Index%20\(NDWI\)%20method%20is%20an%20index,the%20NIR%20and%20green%20bands.&text=For%20information%20about%20other%20multiband,the%20Band%20Arithmetic%20raster%20function](https://pro.arcgis.com/en/pro-app/latest/arcpy/image-analyst/ndwi.htm#:~:text=The%20Normalized%20Difference%20Water%20Index%20(NDWI)%20method%20is%20an%20index,the%20NIR%20and%20green%20bands.&text=For%20information%20about%20other%20multiband,the%20Band%20Arithmetic%20raster%20function) [Accessed 2023].
- ESRI. 2023i. *Pixel value change detection* [Online]. ESRI. Available: <https://pro.arcgis.com/en/pro-app/latest/help/analysis/image-analyst/pixel-value-change-detection.htm> [Accessed 2023].
- ESRI. 2023j. *Project (Data Management)* [Online]. ESRI. Available: <https://pro.arcgis.com/en/pro-app/latest/tool-reference/data-management/project.htm> [Accessed 2023].

- ESRI. 2023k. *Raster Calculator (Spatial Analyst)* [Online]. ESRI. Available: <https://pro.arcgis.com/en/pro-app/3.0/tool-reference/spatial-analyst/raster-calculator.htm> [Accessed 2023].
- ESRI. 2023l. *Reclassify (Spatial Analyst)* [Online]. ESRI. Available: <https://pro.arcgis.com/en/pro-app/latest/tool-reference/spatial-analyst/reclassify.htm> [Accessed 2023].
- ESRI. 2023m. *Sentinel-2 Land Cover Explorer* [Online]. ESRI. Available: <https://livingatlas.arcgis.com/landcoverexplorer/#mapCenter=147.511%2C-19.611%2C10&mode=step&timeExtent=2017%2C2022&year=2019> [Accessed 2023].
- FLORES-ANDERSON, A. I., HERNDON, K. E., THAPA, R. B. & CHERRINGTON, E. 2019. The SAR handbook: Comprehensive methodologies for forest monitoring and biomass estimation.
- GAO, B.-C. 1996a. NDWI—A normalized difference water index for remote sensing of vegetation liquid water from space. *Remote Sensing of Environment*, 58, 257-266.
- GAO, B.-C. 1996b. NDWI?A Normalized Difference Water Index for Remote Sensing of Vegetation Liquid Water from Space. *Remote Sensing of Environment*, 58, 257-266.
- GEOSCIENCE AUSTRALIA. 2015. *Digital Elevation Model (DEM) of Australia derived from LiDAR 5 Metre Grid* [Online]. Geoscience Australia. Available: <https://ecat.ga.gov.au/geonetwork/srv/eng/catalog.search#/metadata/89644> [Accessed 2023].
- GIS APPL. IN HYDROL. MODEL. & REMOTE SENS. 2021a. SNAP for Flood Mapping with Sentinel-1 SAR Image, Part 1/4. YouTube: @SWOT_to_SWAT.
- GIS APPL. IN HYDROL. MODEL. & REMOTE SENS. 2021b. SNAP for Flood Mapping with Sentinel-1 SAR Image, Part 2/4. YouTube: @SWOT_to_SWAT.
- GIS APPL. IN HYDROL. MODEL. & REMOTE SENS. 2021c. SNAP for Flood Mapping with Sentinel-1 SAR Image, Part 3/4. YouTube: @SWOT_to_SWAT.
- GIS APPL. IN HYDROL. MODEL. & REMOTE SENS. 2021d. SNAP for Flood Mapping with Sentinel-1 SAR Image, Part 4/4. YouTube: @SWOT_to_SWAT.
- GIS APPL. IN HYDROL. MODEL. & REMOTE SENS. 2023a. SNAP for Flood Mapping with Sentinel-1 SAR Image (Advanced), Part 1/3. YouTube: @SWOT_to_SWAT.
- GIS APPL. IN HYDROL. MODEL. & REMOTE SENS. 2023b. SNAP for Flood Mapping with Sentinel-1 SAR Image (Advanced), Part 2/3. YouTube: @SWOT_to_SWAT.
- GIS APPL. IN HYDROL. MODEL. & REMOTE SENS. 2023c. SNAP for Flood Mapping with Sentinel-1 SAR Image (Advanced), Part 3/3. YouTube: @SWOT_to_SWAT.
- GUPTA, D. K., PRASHAR, S., SINGH, S., SRIVASTAVA, P. K. & PRASAD, R. 2022. Chapter 1 - Introduction to RADAR remote sensing. In: SRIVASTAVA, P. K., GUPTA, D. K., ISLAM, T., HAN, D. & PRASAD, R. (eds.) *Radar Remote Sensing*. Elsevier.
- HERNANDEZ-SUAREZ, J. S., NEJADHASHEMI, A. P., FERRIBY, H., MOORE, N., BELTON, B. & HAQUE, M. M. 2022. Performance of Sentinel-1 and 2 imagery in detecting aquaculture waterbodies in Bangladesh. *Environmental Modelling & Software*, 157, 105534.
- ICEYE. 2023. *SAR DATA: SEE MORE WITH MODES* [Online]. ICEYE. Available: <https://www.iceye.com/imaging-modes> [Accessed 2023].
- JONES, F. 2016. *Remote-sensing flood data is filling the gaps* [Online]. Bushfire and Natural Hazards CRC. Available: <https://knowledge.aidr.org.au/resources/ajem-jul-2016-remote-sensing-flood-data-is-filling-the-gaps/> [Accessed 2023].
- KAVATS, O., KHRAMOV, D. & SERGIEIEVA, K. 2022a. Surface Water Mapping from SAR Images Using Optimal Threshold Selection Method and Reference Water Mask. *Water*, 14, 4030.
- KAVATS, O., KHRAMOV, D. & SERGIEIEVA, K. 2022b. Surface Water Mapping from SAR Images Using Optimal Threshold Selection Method and Reference Water Mask. *Water* [Online], 14.
- KONAPALA, G., KUMAR, S. V. & KHALIQUE AHMAD, S. 2021. Exploring Sentinel-1 and Sentinel-2 diversity for flood inundation mapping using deep learning. *ISPRS Journal of Photogrammetry and Remote Sensing*, 180, 163-173.
- KUMAR, V., SHARMA, K. V., CALOIERO, T., MEHTA, D. J. & SINGH, K. 2023. Comprehensive overview of flood modeling approaches: A review of recent advances. *Hydrology*, 10, 141.
- LIU, X., SAHLI, H., MENG, Y., HUANG, Q. & LIN, L. 2017. Flood inundation mapping from optical satellite images using spatiotemporal context learning and modest AdaBoost. *Remote Sensing*, 9, 617.

- MA, C., JOHANSEN, K. & MCCABE, M. F. 2022. Monitoring Irrigation Events and Crop Dynamics Using Sentinel-1 and Sentinel-2 Time Series. *Remote Sensing*, 14, 1205.
- MAJOR, T. 2019. *Queensland flooding takes a toll on many as rain brings mixed reactions from farmers* [Online]. Australian Broadcasting Corporation Available: <https://www.abc.net.au/news/rural/2019-02-06/flooding-brings-mixed-reactions-for-north-queensland-farmers/10782034> [Accessed 2023].
- MCVITTIE, A. 2019. *SENTINEL-1: Flood mapping tutorial* [Online]. European Space Agency. Available: https://step.esa.int/docs/tutorials/tutorial_s1floodmapping.pdf [Accessed 2023].
- MOHANTY, M. P. & KARMAKAR, S. 2022. Flood Risk Estimation and Mapping: Present Status and Future Challenges. In: FURZE, J. N., ESLAMIAN, S., RAAFAT, S. M. & SWING, K. (eds.) *Earth Systems Protection and Sustainability: Volume 2*. Cham: Springer International Publishing.
- MRGIS 2020. Sentinel-1 flood mapping with SNAP. YouTube: @MrGIS.
- NATIONAL OCEANIC AND ATMOSPHERIC ADMINISTRATION (NOAA). 2022. *2022 Sea Level Rise Technical Report* [Online]. National Oceanic and Atmospheric Administration. Available: <https://oceanservice.noaa.gov/hazards/sealevelrise/sealevelrise-tech-report.html#step2> [Accessed 2023].
- NOTTI, D., GIORDAN, D., CALÓ, F., PEPE, A., ZUCCA, F. & GALVE, J. P. 2018. Potential and Limitations of Open Satellite Data for Flood Mapping. *Remote Sensing* [Online], 10.
- PARIDA, B. R., PANDEY, A. C., KUMAR, S. & TRIPATHI, G. 2022. Chapter 5 - Comparative flood area analysis based on change detection and binarization methods using Sentinel-1 synthetic aperture radar data. In: SRIVASTAVA, P. K., GUPTA, D. K., ISLAM, T., HAN, D. & PRASAD, R. (eds.) *Radar Remote Sensing*. Elsevier.
- PLANET. 2023a. *Education and Research Program* [Online]. Planet Labs PBC. Available: <https://www.planet.com/markets/education-and-research/> [Accessed 2023].
- PLANET. 2023b. *Real-Time Satellite Monitoring with Planet* [Online]. Planet Labs PBC. Available: <https://www.planet.com/products/monitoring/> [Accessed 2023].
- PLANNING INSTITUTE OF AUSTRALIA. 2022. *VICTORIAN ELECTION 2022* [Online]. Planning Institute of Australia. Available: <https://www.planning.org.au/documents/item/12072> [Accessed 2023].
- RANA, V. K. & SURYANARAYANA, T. M. V. 2019. Evaluation of SAR speckle filter technique for inundation mapping. *Remote Sensing Applications: Society and Environment*, 16, 100271.
- SHASTRY, A., CARTER, E., COLTIN, B., SLEETER, R., MCMICHAEL, S. & EGGLESTON, J. 2023. Mapping floods from remote sensing data and quantifying the effects of surface obstruction by clouds and vegetation. *Remote Sensing of Environment*, 291, 113556.
- SOUZA, W. D., REIS, L. G., RUIZ-ARMENTEROS, A. M., VELEDA, D., RIBEIRO NETO, A., FRAGOSO JR, C. R., CABRAL, J. J. & MONTENEGRO, S. M. 2022. Analysis of Environmental and Atmospheric Influences in the Use of SAR and Optical Imagery from Sentinel-1, Landsat-8, and Sentinel-2 in the Operational Monitoring of Reservoir Water Level. *Remote Sensing* [Online], 14.
- SPRINGER NATURE. 2023. *Table 2 Overview of the Köppen-Geiger climate classes including the defining criteria* [Online]. Springer Nature Limited. Available: <https://www.nature.com/articles/sdata2018214/tables/3> [Accessed 2023].
- THE EUROPEAN SPACE AGENCY. 2023. *Sentinel Online - Level-1 Radiometric Calibration* [Online]. The European Space Agency. Available: <https://sentinels.copernicus.eu/web/sentinel/radiometric-calibration-of-level-1-products> [Accessed 2023].
- THE STATE OF QUEENSLAND. 2022. *Water Monitoring Information Portal* [Online]. The State of Queensland. Available: <https://water-monitoring.information.qld.gov.au/> [Accessed 2023].
- THE STATE OF QUEENSLAND. 2023. *Burdekin drainage basin* [Online]. The State of Queensland (Department of Environment and Science). Available: <https://wetlandinfo.des.qld.gov.au/wetlands/facts-maps/basin-burdekin/> [Accessed 2023].
- WALE, P. B., SIVASANKAR, T., MISHRA, V. N. & SANYAL, R. 2022. Chapter 11 - Flood inundation mapping from synthetic aperture radar and optical data using support vector machine: a case study from Kopili River basin during Cyclone Amphan. In: SRIVASTAVA, P. K., GUPTA, D. K., ISLAM, T., HAN, D. & PRASAD, R. (eds.) *Radar Remote Sensing*. Elsevier.

XU, C., QU, J. J., HAO, X. & WU, D. 2020. Monitoring Surface Soil Moisture Content over the Vegetated Area by Integrating Optical and SAR Satellite Observations in the Permafrost Region of Tibetan Plateau. *Remote Sensing* [Online], 12.

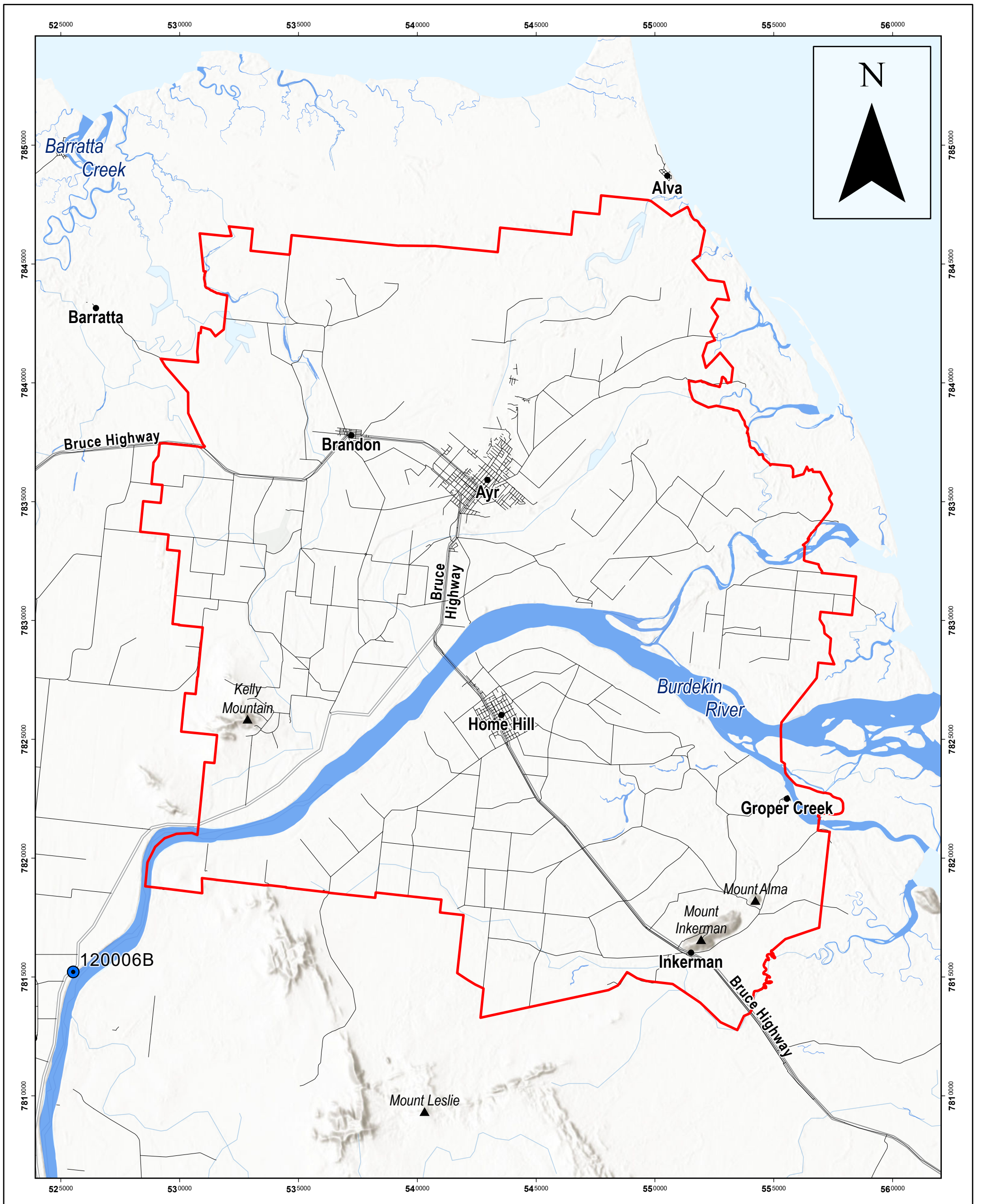
I acknowledge the use of OpenAI in aiding in the planning, editing, and proofreading of my thesis.

OpenAI. (2023). *ChatGPT* (Oct 24 version) [Large language model]. <https://chat.openai.com/chat>

APPENDIX A

Area of Interest (AOI)

An A3 map illustrating the geographic location of the area of interest (AOI) for the study.



Area of Interest (AOI)

0 2.5 5 km

Scale: 1:150,000

Legend

- Clare River Gauge Station
- Populated places
- ▲ Peaks
- Roads
- Rivers/Creeks
- Area of interest (AOI)

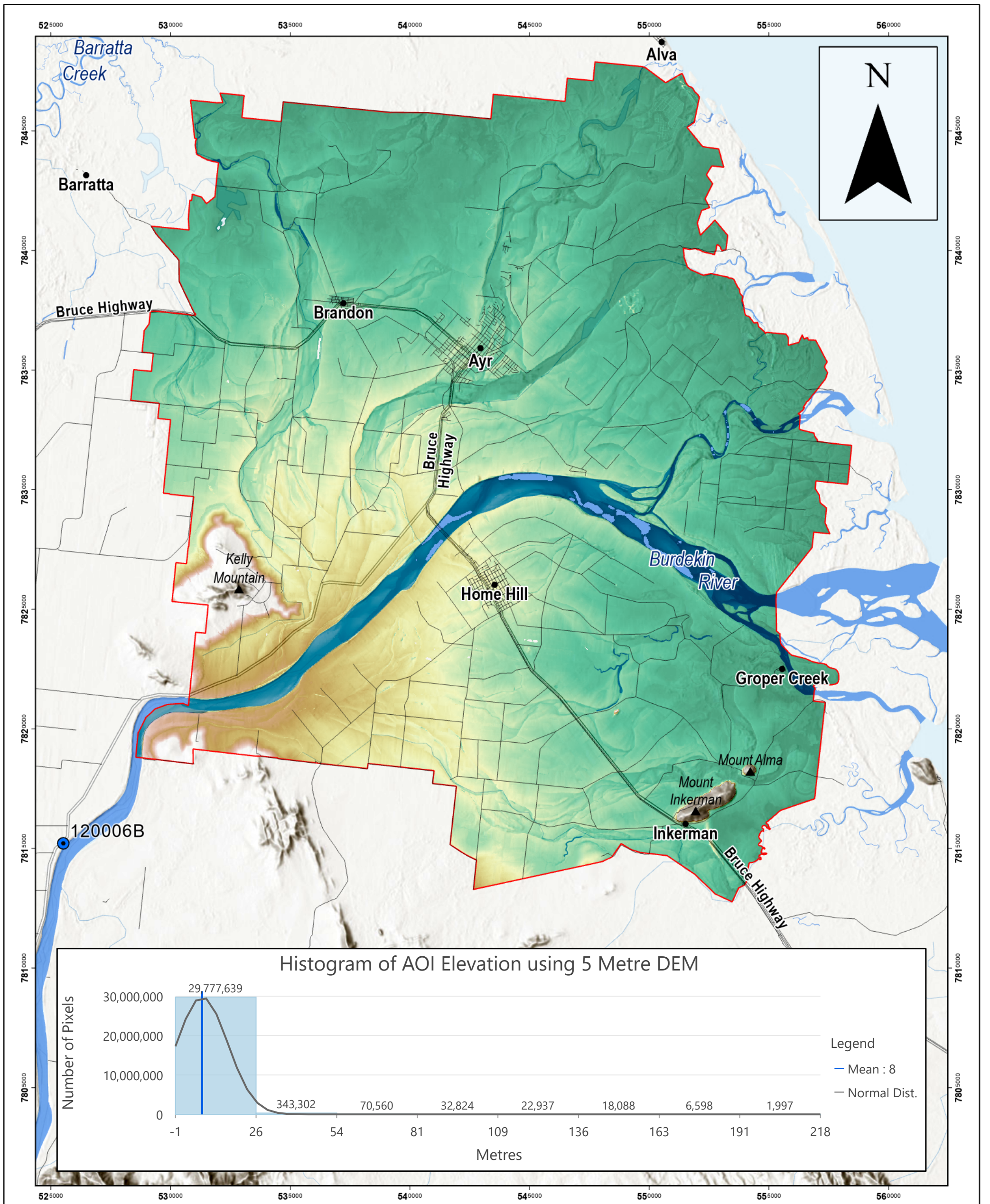
Spatial Reference
 Name: GDA 1994 MGA Zone 55
 Date: 27/02/2024 3:41 PM
 Author: Myles Burt (burt0194)
 Data Sources: Flinders University, QSpatial

Department of Resources, Dept. of Environment and Science,
 Esri, TomTom, Garmin, Foursquare, METI/NASA, USGS,
 Earthstar Geographics, Esri, Geoscience Australia, NASA, NGA,
 USGS

APPENDIX B

Elevation of AOI

An A3 map illustrating the elevation of the area of interest (AOI) for the study using a 5 metre Digital Elevation Model (DEM).



Elevation of AOI

0 2.5 5 km

Scale: 1:150,000

Legend

- Clare River Gauge Station
- Populated places
- ▲ Peaks
- Roads
- ▬ Rivers/Creeks
- Area of interest (AOI)
- Elevation (metres)**
- 218.199
- -0.967

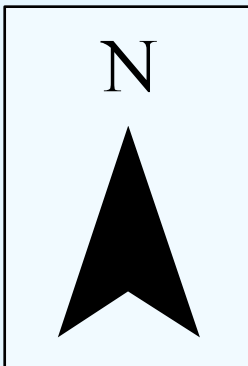
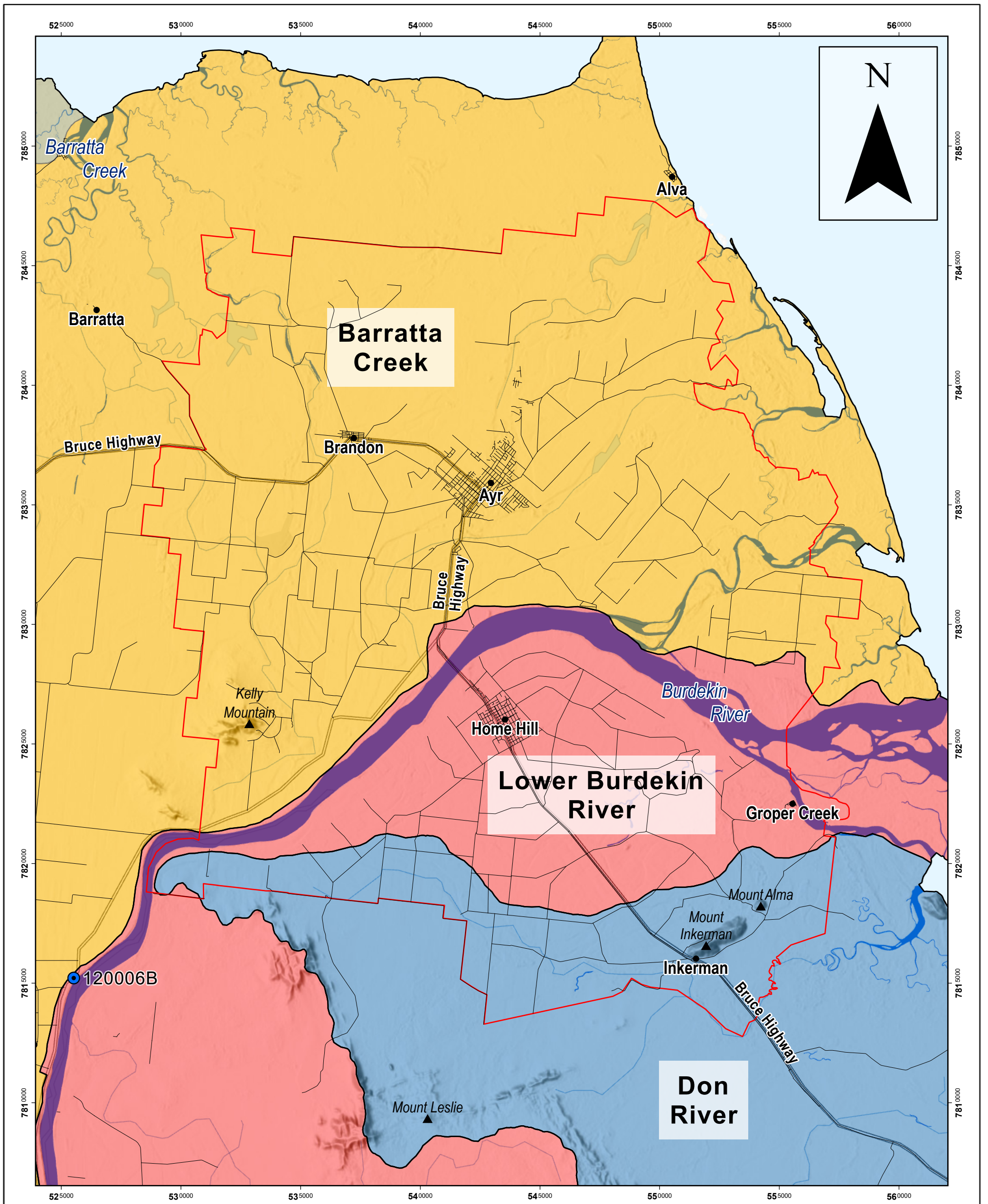
Spatial Reference
 Name: GDA 1994 MGA Zone 55
 Date: 27/02/2024 3:49 PM
 Author: Myles Burt (burt0194)
 Data Sources: Flinders University, Geoscience Australia (2023), QSpatial

Department of Resources, Dept. of Environment and Science, Esri, TomTom, Garmin, Foursquare, METI/NASA, USGS, Earthstar Geographics, Esri, Geoscience Australia, NASA, NGA, USGS

APPENDIX C

Basins and Sub-Basins within the AOI

An A3 map illustrating the geographic location of the area of interest (AOI) within Basins and Sub-Basin.



Basins and Sub-Basins within the AOI

0 2.5 5 km

Scale: 1:150,000

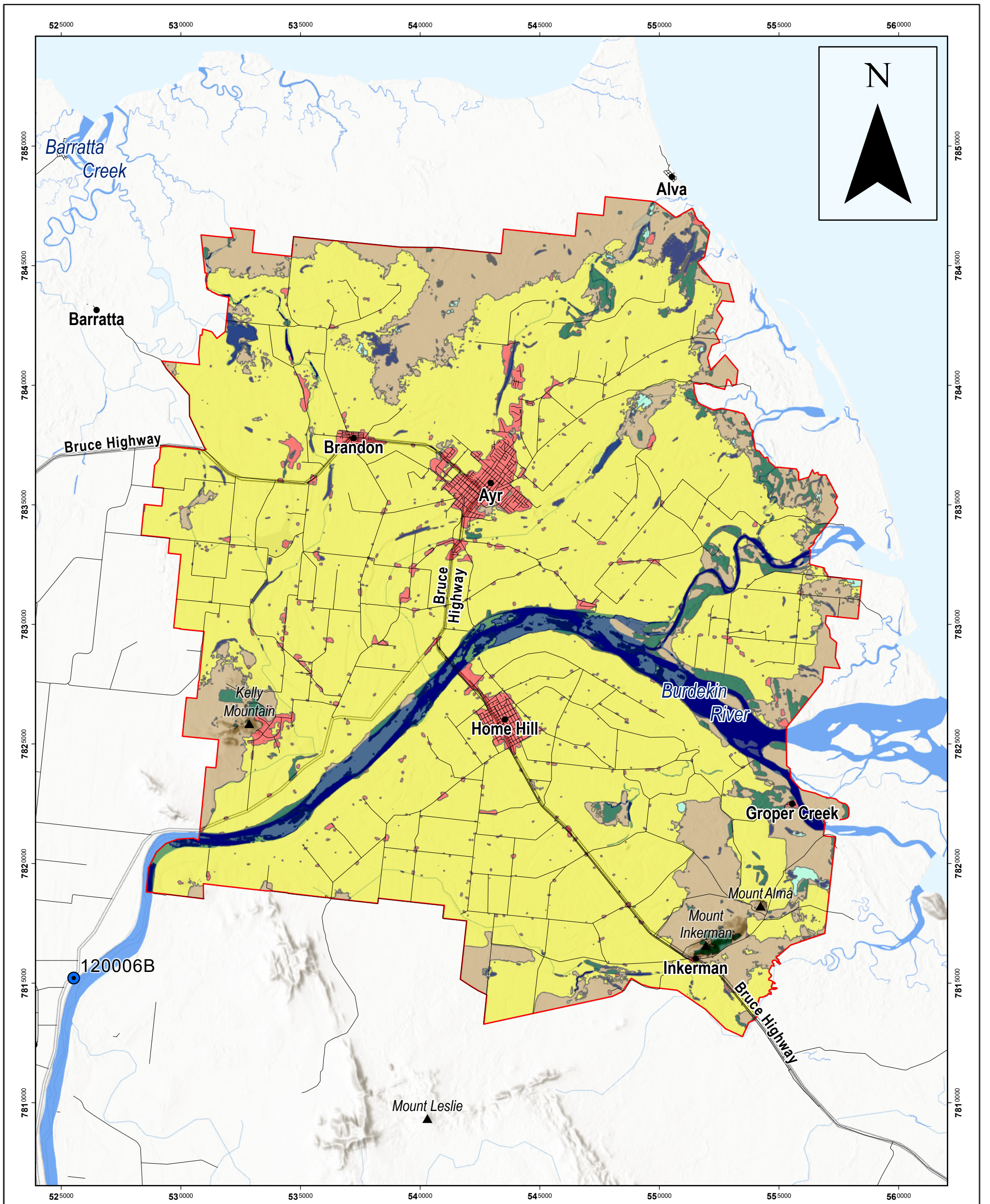
<p>Legend</p> <ul style="list-style-type: none"> ● Clare River Gauge Station ● Populated places ▲ Peaks — Roads — Rivers/Creeks 	<ul style="list-style-type: none"> Area of interest (AOI) Drainage Basins and their Sub-Basins Burdekin Basin — Lower Burdekin River 	<ul style="list-style-type: none"> Don Basin — Don River Haughton Basin — Barratta Creek — Haughton River
---	---	---

Spatial Reference
 Name: GDA 1994 MGA Zone 55
 Date: 27/02/2024 3:44 PM
 Author: Myles Burt (burt0194)
 Data Sources: Flinders University, Australian Bureau of Statistics (2023), QSpatial
 Department of Resources, Dept. of Environment and Science, Esri, TomTom, Garmin, Foursquare, METI/NASA, USGS, Earthstar Geographics, Esri, Geoscience Australia, NASA, NGA, USGS

APPENDIX D

Land Use within AOI using 2019 Land Use / Land Cover Classification Data from Sentinel-2

An A3 map illustrating the land use / land cover classified areas by ESRI using Sentinel-2 within the area of interest (AOI).



Land Use within AOI using 2019 Land Use / Land Cover Classification Data from Sentinel-2

0 2.5 5 km

Scale: 1:150,000

Legend

- | | | |
|---------------------------|------------------------|-------------|
| Clare River Gauge Station | Area of interest (AOI) | Crops |
| Populated places | Land Use | Built Area |
| Peaks | Water | Bare Ground |
| Roads | Trees | Rangeland |
| Rivers/Creeks | Flooded Vegetation | |

Spatial Reference

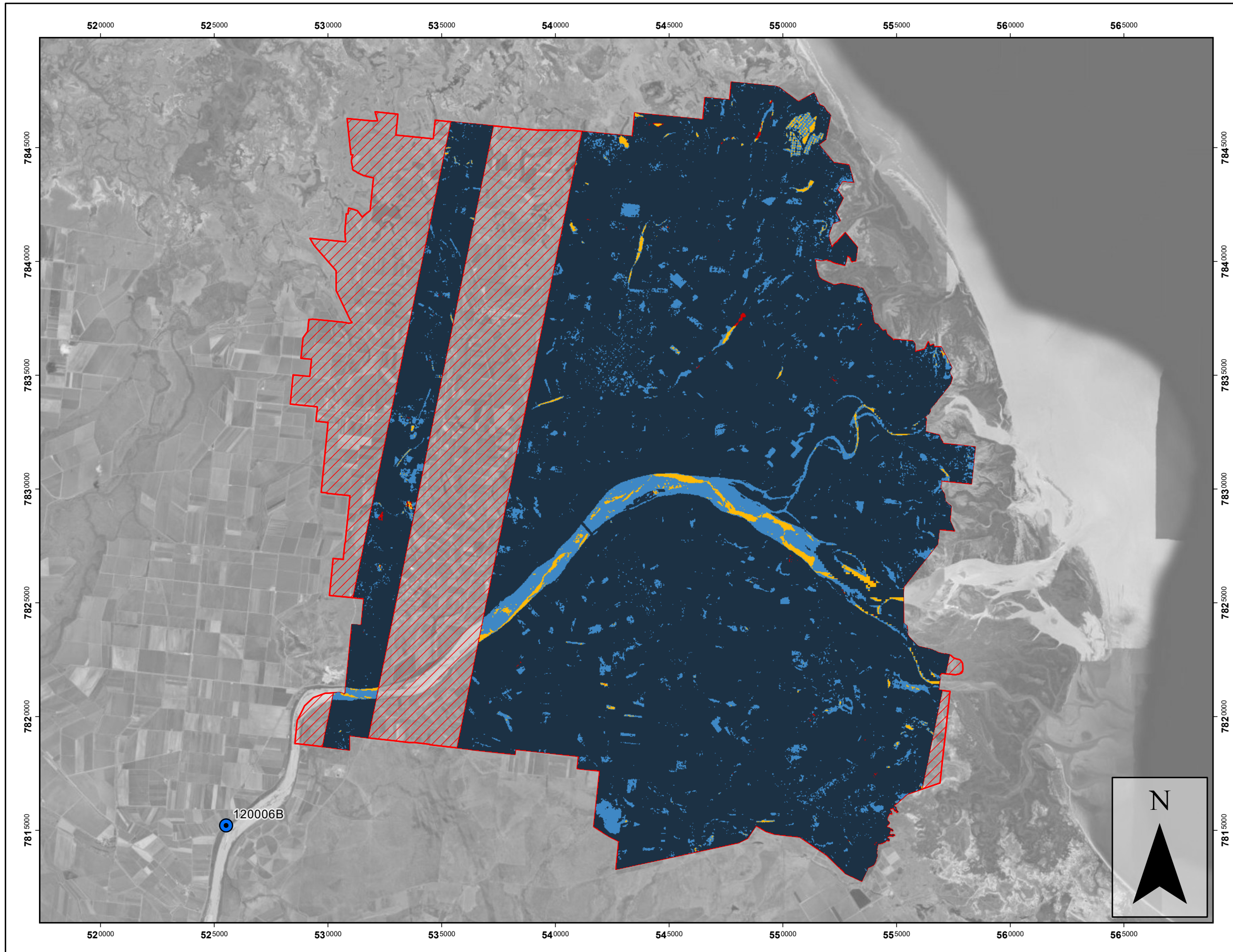
Name: GDA 1994 MGA Zone 55
 Date: 27/02/2024 3:51 PM
 Author: Myles Burt (burt0194)
 Data Sources: Flinders University, ESRI, Impact Observatory, Microsoft, QSpatial

Department of Resources, Dept. of Environment and Science, Esri, TomTom, Garmin, Foursquare, METI/NASA, USGS, Earthstar Geographics, Esri, Geoscience Australia, NASA, NGA, USGS

APPENDIX E

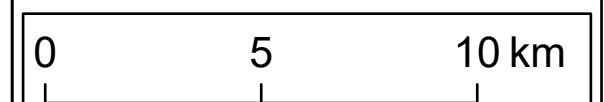
Classified Areas of Change Detected in SAR rasters between Pre-flood and Flood

An A3 map illustrating the classified areas of always dry, flood, false change, and always wet that have been identified by employing SAR flood detection methods within the area of interest (AOI).



- Legend**
- Clare River Gauge Station
 - Area of interest (AOI)
 - Areas where optical data was unavailable
- Classifications**
- Always Dry
 - Flood
 - False Change (Dry in Pre-Flood)
 - Always Wet

Classification	Area (Km2)	Percentage
Always Dry	535.9	91
Flood	44.7	8
False Change	0.4	0
Always Wet	6.3	1



Scale: 1:175,000

Spatial Reference
 Name: GDA 1994 MGA Zone 55
 Date: 24/10/2023 10:53 PM
 Author: Myles Burt (burt0194)
 Data Sources: Flinders University, The State of Queensland - Department of Resources (2023), Alaska Satellite Facility (2023)

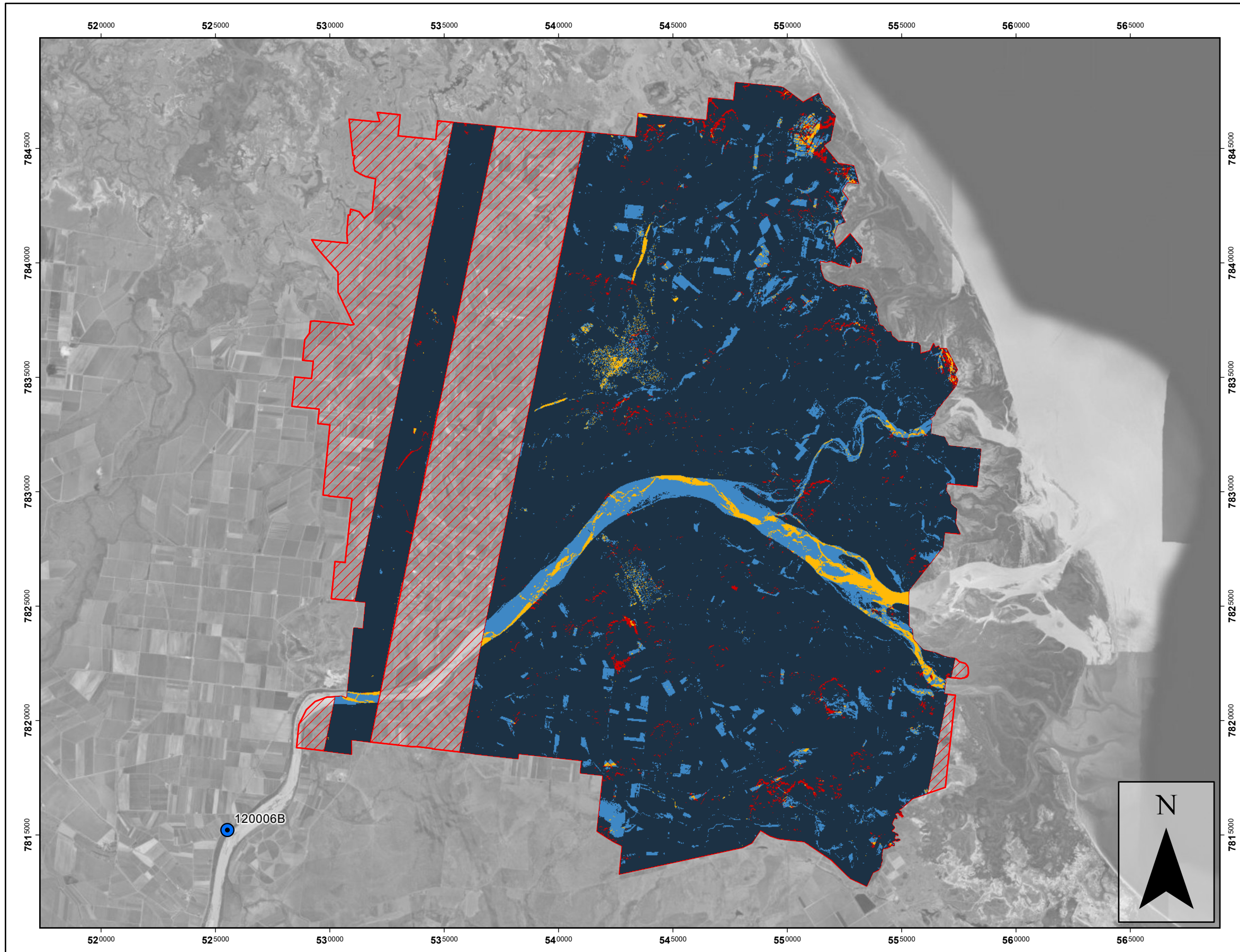
ESRI Credits: Earthstar Geographics

Classified Areas of Change Detected in SAR rasters between Pre-flood and Flood

APPENDIX F

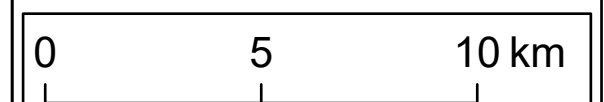
Classified Areas of Change Detected in NDWI rasters between Pre-flood and Flood

An A3 map illustrating the classified areas of always dry, flood, false change, and always wet that have been identified by employing NDWI flood detection methods within the area of interest (AOI).



- Legend**
- Clare River Gauge Station
 - Area of interest (AOI)
 - Areas where optical data was unavailable
- Classifications**
- Always Dry
 - Flood
 - False Change (Dry in Pre-Flood)
 - Always Wet

Classification	Area (Km2)	Percentage
Always Dry	518	89
Flood	49.2	8
False Change	6.6	1
Always Wet	10.5	2



Scale: 1:175,000

Spatial Reference
 Name: GDA 1994 MGA Zone 55
 Date: 24/10/2023 10:55 PM
 Author: Myles Burt (burt0194)
 Data Sources: Flinders University, The State of Queensland - Department of Resources (2023), Alaska Satellite Facility (2023)

ESRI Credits: Earthstar Geographics

Classified Areas of Change Detected in NDWI rasters between Pre-flood and Flood